

Bar formation and evolution in disc galaxies with gas and a triaxial halo: Morphology, bar strength and halo properties

E. Athanassoula^{1*}, Rubens E. G. Machado^{1,2}, S.A. Rodionov^{1,3}

¹*Aix Marseille Université, CNRS, LAM (Laboratoire d'Astrophysique de Marseille) UMR 7326, 13388, Marseille, France*

²*Instituto de Astronomia, Geofísica e Ciências Atmosféricas, Universidade de São Paulo, R. do Matão 1226, 05508-090 São Paulo, Brazil*

³*Sobolev Astronomical Institute, St. Petersburg State University, Universitetskij pr. 28, 198504 St. Petersburg, Stary Peterhof, Russia*

Accepted ???? ???? Received ???? ???? ??

ABSTRACT

We follow the formation and evolution of bars in N-body simulations of disc galaxies with gas and/or a triaxial halo. We find that both the relative gas fraction and the halo shape play a major role in the formation and evolution of the bar. In gas-rich simulations, the disc stays near-axisymmetric much longer than in gas-poor ones, and, when the bar starts growing, it does so at a much slower rate. Due to these two effects combined, large-scale bars form much later in gas-rich than in gas-poor discs. This can explain the observation that bars are in place earlier in massive red disc galaxies than in blue spirals. We also find that the morphological characteristics in the bar region are strongly influenced by the gas fraction. In particular, the bar at the end of the simulation is much weaker in gas-rich cases. The quality of our simulations is such as to allow us to discuss the question of bar longevity because the resonances are well resolved and the number of gas particles is sufficient to describe the gas flow adequately. In no case did we find a bar which was destroyed.

Halo triaxiality has a dual influence on bar strength. In the very early stages of the simulation it induces bar formation to start earlier. On the other hand, during the later, secular evolution phase, triaxial haloes lead to considerably less increase of the bar strength than spherical ones. The shape of the halo evolves considerably with time. We confirm previous results of gas-less simulations that find that the inner part of an initially spherical halo can become elongated and develop a halo bar. However we also show that, on the contrary, in gas rich simulations, the inner parts of an initially triaxial halo can become rounder with time. The main body of initially triaxial haloes evolves towards sphericity, but in initially strongly triaxial cases it stops well short of becoming spherical. Part of the angular momentum absorbed by the halo generates considerable rotation of the halo particles that stay located relatively near the disc for long periods of time. Another part generates halo bulk rotation, which, contrary to that of the bar, increases with time but stays small. Thus, in our models there are two non-axisymmetric components rotating with different pattern speeds, namely the halo and the bar, so that the resulting dynamics have strong similarities to the dynamics of double bar systems.

Key words: methods: N-body simulations – galaxies: evolution – galaxies: haloes – galaxies: kinematics and dynamics – galaxies: structure

1 INTRODUCTION

Bars, weak or strong, are present in the majority of present-day disc galaxies (e.g. de Vaucouleurs et al. 1991; Eskridge et al. 2000; Knapen et al. 2000; Whyte et al. 2002; Marinova & Jogee 2007; Menéndez-Delmestre et al. 2007; Barazza et al. 2008; Aguerrí, Méndez-Abreu, & Corsini 2009; Marinova et al. 2009; Méndez-Abreu et al. 2010; Masters et al. 2011), with an often

quoted fraction of roughly two thirds. They can also be found at higher redshifts (Abraham et al. 1996; van den Bergh et al. 1996; Abraham et al. 1999; Elmegreen et al. 2004; Jogee et al. 2004), although there they constitute a smaller fraction of the disc galaxies than at low redshifts (Sheth et al. 2008; Nair & Abraham 2010). A number of observational studies, ranging from in-depth studies of single objects to large surveys, have provided useful information on the morphological, photometrical and kinematical properties of bars (e.g. Sheth et al. 2005; Gadotti et al. 2007; Marinova et al. 2009; Buta et al. 2010; Gadotti 2011;

* E-mail: lia@oamp.fr

Hoyle et al. 2011; Laurikainen et al. 2011; Masters et al. 2011; Simard et al. 2011; Beirão et al. 2012; Martínez-García 2012; Pérez, Aguerrí, & Méndez-Abreu 2012; Wang et al. 2012).

This observational effort was accompanied by a considerable effort with N-body simulations (e.g. Debattista & Sellwood 2000; Athanassoula & Misiriotis 2002; Athanassoula 2002; Athanassoula 2003, hereafter A03; O’Neill & Dubinski 2003; Valenzuela & Klypin 2003; Martínez-Valpuesta et al. 2006; Holley-Bockelmann et al. 2005; Dubinski et al. 2009). Such simulations provided information on the formation and evolution of barred galaxies, on the role of the halo and on the redistribution of angular momentum within the galaxy. They furthermore allowed detailed comparisons with observations. Even so, this simulation work can be considered as the first step, since it has, by necessity, relied on a number of simplifying approximations. In this paper, we will revisit two such approximations, and consider bar formation and evolution in their absence, i.e. in more realistic cases than in previous studies.

One approximation used in the vast majority of previous studies is that initially the halo is spherically symmetric. Yet cosmological simulations (e.g. Dubinski & Carlberg 1991; Jing & Suto 2002; Bailin & Steinmetz 2005; Allgood et al. 2006; Novak et al. 2006; Vera-Ciro et al. 2011; Schneider, Frenk, & Cole 2012) have shown that in cases with no baryons the haloes are strongly triaxial, as could be expected by the fact that the halo shapes can be strongly modified during interactions and mergings (McMillan et al. 2007; Kazantzidis et al. 2004), as well as by the radial orbit instability (Merritt & Aguilar 1985; Barnes, Hut, & Goodman 1986; Dejonghe & Merritt 1988; Aguilar & Merritt 1990; Weinberg 1991; Cannizzo & Hollister 1992; Huss, Jain, & Steinmetz 1999; Boily & Athanassoula 2006; MacMillan, Widrow, & Henriksen 2006; Bellovary et al. 2008)

Yet observations show that present day haloes should be considerably more axisymmetric in the equatorial plane than the above mentioned papers suggest (e.g. Trachternach et al. 2008), while haloes in cosmological simulations including baryons are less triaxial. It is thus necessary to understand the effect of baryons on the evolution of halo shapes in barred galaxies. Aspects of this question have been already addressed in several papers (Dubinski 1994; Gadotti & de Souza 2003; Curir et al. 2006; Berentzen et al. 2006; Berentzen & Shlosman 2006; Athanassoula 2007; Widrow 2008; Debattista et al. 2008; Machado & Athanassoula 2010, hereafter MA10), but a full understanding is still not available.

A second, often used approximation consists in either neglecting the gas component, or modelling it in an oversimplified way. Yet gas has a considerable effect on the evolution of disc galaxies. Its mass may be a small fraction of the total at present, but it has been much more important in the past (e.g. Tacconi et al. 2010). Furthermore, gas, being a cold component, can respond quite strongly to gravitational perturbations. A number of studies including gas have given important insight (e.g. Berentzen et al. 1998; Bournaud & Combes 2002; Berentzen et al. 2003, 2004; Bournaud, Combes, & Semelin 2005; Debattista et al. 2006; Berentzen et al. 2007; Heller, Shlosman, & Athanassoula 2007a,b; Wozniak & Michel-Dansac 2009; Villa-Vargas, Shlosman, & Heller 2010; DeBuhr, Ma & White 2012), but relatively few had a sufficient number of particles (Patsis & Athanassoula 2000), and most of them neglected the physics of the gas, i.e. neglected its multi-phase nature, as well as the related star formation, feedback and cooling. In these simplified cases the amount of gas stays constant during the simulation, so, if the simulation spans several Gyr, the adopted gas fraction is too

low during the first part of the simulation and/or too high during the last part.

Since this paper was submitted, two new papers on related subjects were published. They both use cosmological zoom re-simulations and include gas with a realistic physics. The first one (Kraljic et al. 2012) measures the fraction of disc galaxies that are barred and compares them to observations, while the second one (Scannapieco & Athanassoula 2012) studies bar properties of two bars in Aquarius galaxies.

In the present paper we follow the formation and evolution of a bar in a disc galaxy with a triaxial halo and which includes a gaseous disc component undergoing star formation, feedback and cooling. In Sect. 2 we give information on the numerical aspects of the work. In particular, we describe our use of the GADGET2 code, how the equilibrium initial conditions were derived and what their relevant properties are (Sect. 2.2). Results are given and discussed in Sects. 3 to 7. Sect. 3 gives the evolution with time of the gas fraction and of the general morphology. In Sect. 4 we discuss the evolution of the bar strength with time and in Sect. 5 we enter the debate of whether bars are long-lived or short-lived. In Sect. 6 we present the radial profiles and the time evolution of the halo axial ratios, as well as the kinematics of the halo material. The latter together with the angular momentum redistribution within the galaxy we relate to the bar strength. Interaction between the various non-axisymmetric components is the subject of Sect. 7. We present further discussion of our results in Sect. 8 and conclude in Sect. 9.

2 TECHNIQUES

2.1 Simulations

We use a version of GADGET2 including gas and its physics (Springel, Yoshida, & White 2001; Springel & Hernquist 2002; Springel 2005). The dark matter and the stars are followed by N-body particles and gravity is calculated with a tree code. The code uses an improved SPH method (Springel & Hernquist 2002) and sub-grid physics (Springel & Hernquist 2003). In this approach, each SPH particle represents a region of the ISM containing both cold gas clouds and hot ambient gas, the two in pressure equilibrium.

In the following we use the GADGET2 system of units; i.e. the unit of length is 1 kpc, the unit of mass is $10^{10} M_{\odot}$ and the unit of velocity 1 km/sec. As a result the time unit is 0.98 Gyr. For simplicity, and given the accuracy of all our measurements, we used a time unit of one Gyr. We continued all simulations up to 10 Gyr. This is longer than what is expected for the combined bar formation and evolution phases in real disc galaxies, but allows us to follow fully all secular evolution phases. For comparisons with observed nearby galaxies, however, times between 6 and 8 Gyr may be more appropriate. For this reason we will include in many of our discussions information from both the 6 and the 10 Gyr results. We used a softening length of 50 pc for all components and an opening angle for the tree-code of 0.5.

GADGET2 offers the possibility of using several types of particles for the various components of the galaxy. In the following we will use four types, namely: HALO, DISK, GAS and STARS. The DISK particles represent stars already present in the initial conditions and their number remains constant throughout the simulation. But as the simulation evolves, gas particles give rise to new stars, via star formation, so that both the DISK particles and the STAR particles represent the stars of the galaxy. To distinguish between

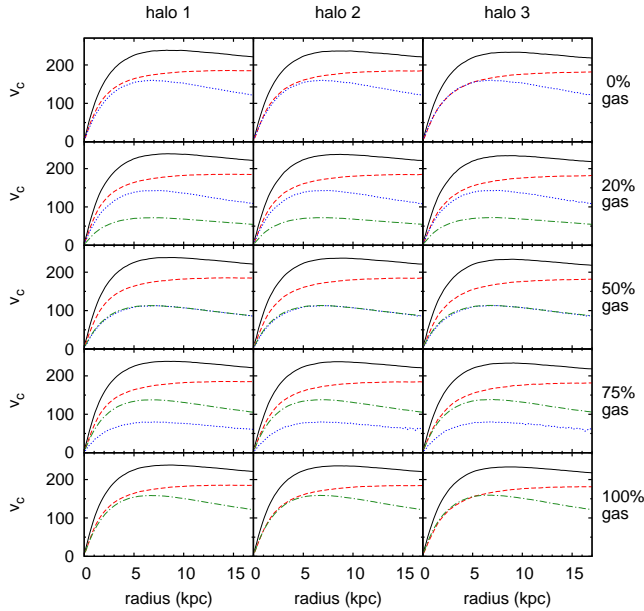


Figure 1. Circular velocity curves of the initial conditions ($t = 0$): total (solid lines, black in the online version), halo (dashed, red on the online version), disk (dotted, blue in the online version) and gas (dot-dashed, green in the online version). The three columns, from left to right, correspond to the three haloes used in this paper, namely halo 1, halo 2 and halo 3. Each row corresponds to a different initial gas fraction (calculated as the fraction of gas in the disc component).

the different components, we will use in the following the words DISK and STARS when we talk about the corresponding GADGET2 components, the words ‘stellar disc’ when we refer to all stellar particles in the galactic disc (i.e. when we refer to both the DISK and STARS particles together) and the word ‘disc’ when we refer to all components in the disc, i.e. DISK, STARS and GAS. The DISK component may be thought of as representing an older stellar population, whereas the STARS particles represent a mix of stars ranging in age from very young to as old as the simulation time. The gas and halo particles, where no confusion is possible, will be simply referred to as ‘gas’ and ‘halo’, respectively.

2.2 Initial conditions

Information on the initial conditions of all models used in this paper is given in Table 1. The first four columns give the run number, the halo which is used and its b/a and c/a axial ratios, respectively. The semi-major axes a , b and c are placed along the x , y and z axes respectively. The fifth column gives the fraction of gas in the disc component and the sixth one gives the number of particles in the gas component.

The initial conditions have been built using the iterative method (Rodionov, Athanassoula & Sotnikova 2009), and, more specifically, its extension to include a gaseous component (Rodionov & Athanassoula 2011). We make a series of short constrained iterative steps to build each component in near-equilibrium in the total galactic potential. In this way we avoid transients which could affect the instabilities under study. In the triaxial models, both the stellar and the gaseous disc have an elliptical shape (see Rodionov et al. 2009 for details). The circular velocity curves of the initial conditions are shown in Fig. 1. They are essentially the

same for all models, as required for a study of the effect of gas fraction and halo triaxiality.

It should be stressed that a simulation from the present work can not be directly compared with a simulation from MA10 with the same halo initial axial ratios, because of the difference in how the initial conditions were made. Indeed in MA10 we first prepared an equilibrium halo model with the desired axial ratio. Then a disc was grown in this halo, which brings about an axisymmetrisation of the latter component of the order of half its final axisymmetrisation. So the halo potential that the bar feels as it grows is considerably less triaxial than that of the initial halo model. For example, when, in MA10, we started with a halo model of axial ratios $b/a = 0.8$ and $c/a = 0.6$, we obtained after the disc was introduced a rounder halo with an axial ratio b/a of ~ 0.9 . This is not the case here, where the disc is built in equilibrium within the halo having the prescribed axial ratio. So if we want to compare one of our simulations with that particular MA10 simulation, we would have to use one with $b/a = 0.9$ and not 0.8. Further differences concern the disc, whose shape here is obtained by the iterative method in its search for near-equilibrium.

The initial azimuthally averaged density distribution of the stellar disc is given by

$$\rho_d(R, z) = \frac{M_d}{4\pi h^2 z_0} \exp(-R/h) \operatorname{sech}^2\left(\frac{z}{z_0}\right), \quad (1)$$

where R is the cylindrical radius, M_d is the disc mass, h is the disc radial scale length and z_0 is the disc vertical scale thickness. The radial scale length is $h = 3$ kpc and the scale height is $z_0 = 0.6$ kpc. For the gas we adopt the same radial profile and the same scale length. This is necessary in order to be able to make sequences of models where only the gas fraction changes and all the remaining parameters and quantities are the same. The gas scale height is considerably smaller than that of the stars and its precise value is set by the hydrostatic equilibrium achieved during the iterative calculation of the initial conditions (Rodionov & Athanassoula 2011). The total disc mass (stellar plus gaseous) is always $M_d = 5 \times 10^{10} M_\odot$.

When creating the initial conditions we impose a radial velocity dispersion for the DISK particles, $\sigma_R(R)$, of

$$\sigma_R(R) = 100 \cdot \exp(-R/3h) \text{ km s}^{-1}. \quad (2)$$

All haloes have been built so as to have, within the allowed accuracy, the same spherically averaged initial radial profile, namely

$$\rho_h(r) = \frac{M_h}{2\pi^{3/2}} \frac{\alpha}{r_c} \frac{\exp(-r^2/r_c^2)}{r^2 + \gamma^2}, \quad (3)$$

where r is the radius, M_h is the mass of the halo and γ and r_c are the halo core and cut-off radii. The parameter α is a normalisation constant defined by

$$\alpha = [1 - \sqrt{\pi} \exp(q^2) (1 - \operatorname{erf}(q))]^{-1}, \quad (4)$$

where $q = \gamma/r_c$ (Hernquist 1993). In all simulations we take $\gamma = 1.5$ kpc, $r_c = 30$ kpc and $M_h = 2.5 \times 10^{11} M_\odot$.

This model has several advantages. Compared to observations, its rotation curve (Fig. 1) has a realistic shape. We have also avoided a strong cusp in the centre, in good agreement with observations (e.g. de Blok et al. 2001; de Blok & Bosma 2002; de Blok, Bosma & McGaugh 2003; Simon et al. 2003; Kuzio de Naray et al. 2006; Kuzio de Naray, McGaugh & de Blok 2008; de Blok et al. 2008; Oh et al. 2008; Battaglia et al. 2008; de Blok 2010; Walker & Peñarrubia 2011; Amorisco & Evans 2012; Peñarrubia et al. 2012). Finally, this model has been used in a number of previous studies, on which we were able to rely here. For

example, Athanassoula (2002) determined the number of particles which we need to have in a halo of this type in order to describe its resonances adequately for the evolution. This necessitated the calculation of a large number of orbits in order to determine when they get kicked in or out of resonance by particle noise. As this was done for a range of softening values (Athanassoula, unpublished), we were able to rely here on these results.

At the request of the referee, we compare here quantitatively our halo profile with that of a cosmologically motivated NFW profile (Navarro, Frenk & White 1996). The main difference of course is that the NFW profile has a cusp in the innermost parts, while ours has a core. As already mentioned above, we made this choice in order to be in agreement with observations. To compare the two profiles at larger radii, we tried fitting our profile with an NFW profile in the region one to 20 kpc, but we could get an acceptable fit only for large values of the concentration parameter, $c_{200} > 30$, which are much larger than the cosmologically motivated values. This comparison, however, is not fair. Indeed, in our iterative solution the disc and halo are built in equilibrium within each other, while the NFW profile is a stand-alone component. For a fair comparison we need to calculate the adiabatic contraction of a cosmologically motivated NFW halo ($M_{200} = 10^{12} M_{\odot}$ and $c_{200} = 8.07$, see Prada et al. 2012), due to the disc we adopted (eq. (3)) and compare its cumulative mass profile to that of our halo profile. We used the method described in Gnedin et al. (2004) and found an agreement better than, or of the order of 10% in the region 3 to 35 kpc, i.e. everywhere except the innermost region (as could be expected because we – wilfully – used a core while the NFW profile has a cusp) and the outermost region beyond 35 kpc, where our gradual cut-off becomes important. Note, however, that moving this cut-off outwards by a factor of three does not change the results of the simulations significantly for spherically symmetric haloes. Thus we can conclude that our results are not incompatible with a cosmologically motivated NFW profile, within a radius range of more than 10 disc scale lengths, which includes the main bar resonances, and which excludes of course the central cusp/core region.

In all simulations presented here the halo is represented by 10^6 particles and the mass of each halo particle is $m_{halo} = 2.5 \times 10^5 M_{\odot}$. The total disc mass is always one fifth of the total halo mass, but the disc particles are initially distributed in two components: the gas particles and the DISK particles. Because each set of three models has a different fraction of the total disc mass in the form of gas, the numbers of DISK and gas particles are different. This is made in such a way that the mass of each gas particle is always the same in all initial conditions: $m_{gas} = 5 \times 10^4 M_{\odot}$. Likewise, $m_{DISK} = 2.5 \times 10^5 M_{\odot}$ is the same in all simulations. The DISK and halo mass resolutions are the same, but the gas mass is more resolved. Indeed preliminary test simulations showed that a high number of gas particles is necessary in order to describe reasonably well the gas component (see also Patsis & Athanassoula 2000), considerably more than what has been used in most previous such studies. To make sure that this number of particles is sufficient we ran one simulation (simulation 111 in Table 1) four more times, with one quarter, one half, double and quadruple the number of particles for all components, i.e. reaching two million of gas particles. We also re-ran simulation 106 with five times more stellar and dark matter particles and 20 times as many gas particles, i.e. reaching 4 million gas particles. Comparing all these runs showed us that for the global properties discussed here, the resolution we have adopted is well sufficient.

Table 1. Properties of model initial conditions

run	halo	b/a	c/a	gas fraction	N_{gas}
101	1	1.0	1.0	0.0	0
102	2	0.8	0.6	0.0	0
003	3	0.6	0.4	0.0	0
106	1	1.0	1.0	0.2	2×10^5
109	2	0.8	0.6	0.2	2×10^5
110	3	0.6	0.4	0.2	2×10^5
111	1	1.0	1.0	0.5	5×10^5
114	2	0.8	0.6	0.5	5×10^5
115	3	0.6	0.4	0.5	5×10^5
116	1	1.0	1.0	0.75	7.5×10^5
117	2	0.8	0.6	0.75	7.5×10^5
118	3	0.6	0.4	0.75	7.5×10^5
119	1	1.0	1.0	1.	1×10^6
120	2	0.8	0.6	1.	1×10^6
121	3	0.6	0.4	1.	1×10^6

2.3 Analysis

In Athanassoula & Misiriotis (2002) and MA10 we described a number of techniques for measuring quantities relevant to the particle distributions. Unless stated otherwise, we will use them also here and refer the reader to the above mentioned two papers for a full description.

2.3.1 Halo shape

To measure the axial ratios of the halo, we first calculate the local halo density at the position of each halo particle using its distance to its nearest neighbours, then sort out these particles with respect to this local density, divide them in bins of equal particle number and then calculate the axial ratios from the eigenvalues of the inertia tensor calculated within each bin. In this way we avoid the bias which would have been introduced had we sorted the particles with respect to distance from the centre, as initially pointed out by Athanassoula & Misiriotis (2002). For each bin we also calculate the mass weighted mean radius. If we wish to have information within a given range of radii, we take the average of those bins whose mean radius is included in the chosen range.

2.3.2 Bar strength

The strength of the bar is not a uniquely defined quantity, and in fact any function of the bar mass, axial ratio and length can be considered. Thus many different definitions have been so far used. Here we will use a particularly straightforward one, based on the Fourier components of the bi-dimensional mass distribution

$$a_m(R) = \sum_{i=0}^{N_R} m_i \cos(m\theta_i), \quad m = 0, 1, 2, \dots \quad (5)$$

$$b_m(R) = \sum_{i=0}^{N_R} m_i \sin(m\theta_i), \quad m = 1, 2, \dots \quad (6)$$

where N_R is the number of particles inside a given annulus around the cylindrical radius R , m_i is the mass of particle i and θ_i its

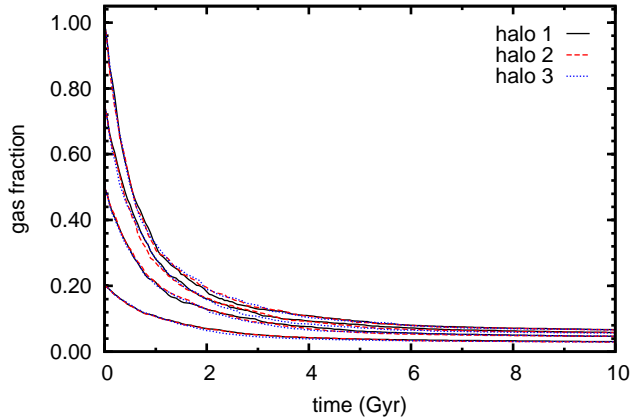


Figure 2. Fraction of gas in the disc component as a function of time, for all simulations discussed here. We use different line styles and colours for simulations with different haloes, as given in the upper right corner. It is clear that the gas fraction at any given time depends strongly on the initial gas fraction, but hardly on the halo initial ellipticity.

Table 2. Fraction of gas in the disc for different times (in Gyr, left column)

time	gas fraction			
0	20%	50%	75%	100%
2	7%	13%	16%	19%
5	4%	6%	8%	9%
10	3%	5%	6%	7%

azimuthal angle. The $a_m(R)$ and $b_m(R)$, however, are a function of the cylindrical radius, while we need to characterise the bar strength by a single number at every time and for every simulation. We will thus measure the bar strength by the maximum amplitude of the relative $m = 2$ component, namely

$$A_2 = \max \left(\frac{\sqrt{a_2^2 + b_2^2}}{a_0} \right). \quad (7)$$

The cylindrical radius at which this maximum occurs will be denoted by R_{max} . We verified that this measure of the bar strength gives qualitatively similar results to those of the other measures used e.g. in MA10 or A03, while being more straightforward to implement for simulations with gas, where considerable spiral structure can be present and the form of the $A_2(R)$ curves can be considerably perturbed.

3 GLOBAL EVOLUTION

3.1 Gas fraction

Fig. 2 displays the evolution of the gas fraction with time. It shows that this decreases with time, as expected because of the star formation. This decrease is quite steep during the first couple of Gyr, when the gas fraction is still high, and then flattens out. Fig. 2 also shows that the shape of the halo hardly, if at all, influences the total amount of stars formed and therefore the amount of gas left at any time.

Table 2 gives the fraction of gas in the disc at given times during the simulation as a function of the initial corresponding gas

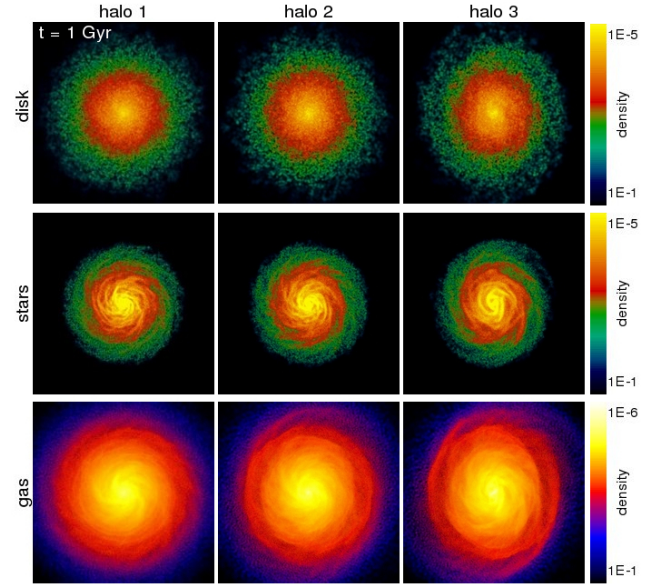


Figure 3. Face-on views at $t = 1$ Gyr for three of our simulations with an initial gas fraction of 50%. The three columns correspond to the three haloes (from left to right halo 1, halo 2 and halo 3, and the three rows (from top to bottom) to the DISK, STARS and gas components, respectively. Colour coding is according to the local projected density of the plotted component, as given by the colour bars to the right of the plot. The size of each square box corresponds to 40 kpc.

fraction value. These values were obtained as mean values over all the runs which start off at $t = 0$ with the given value of the initial gas fraction. The initial values cover the whole range of 0 to 100%, and becomes 0 to 9% at $t = 5$ Gyr and 0 to 7% at $t = 10$ Gyr. These values are in good agreement with values observed for disc-like galaxies at intermediate redshifts, as well as with the gas content of nearby spirals (Erb et al. 2006; Leroy et al. 2008; Daddi et al. 2010; Tacconi et al. 2010; Conselice et al. 2012).

3.2 Early evolution times

Let us first briefly describe the morphology of the disc components during the early evolution ($0 < t < 1$ Gyr), i.e. at times when the bar is not yet visible.

The initial conditions of our simulations were set up so that all components are as near equilibrium as possible in the common potential. Therefore, in the cases where the halo is far from axisymmetric, the DISK and gas components are also initially elongated, but less so than the halo, with initial b/a values in the relatively outer parts roughly in the range 0.95 – 0.9 and 0.9 – 0.8, for halo 2 and halo 3, respectively. This lasts at least during the first Gyr (Fig. 3) and in many cases considerably longer.

Fig. 3 displays the morphology of the three components at $t = 1$ Gyr for the three simulations with 50% initial gas. This gives a fair idea of what happens for other initial gas fractions, since the latter does not influence much this early evolution, except of course for the amount of stars formed and the strength of the spiral structure in the stellar component.

The DISK component preserves roughly its elongation all through the early evolution time. Apart from that, it shows no structure, except, in the case of halo 3, for some faint spiral arms. The gas component also roughly preserves its elongation during these times. It develops strong spiral arms of high multiplicity and in a

few cases an inner oval structure. The STARS component forms inside out, i.e. stars form initially at small radii, as expected from the fact that the gas density is higher in the inner parts. Strong spiral arms can be seen in this component also, whose positions and sizes correspond well to those of their gaseous counterparts.

3.3 Global trends

Figs. 4 and 5 display the face-on views of the baryonic component of our simulations. The halo component is not included in the plots and its discussion will be left for Sect. 6. Each figure should be viewed as three blocks of three columns each. The first block of three columns corresponds to the DISK, the second block to the STARS, and the last one to the gas. The three columns in each block correspond to simulations with the haloes halo 1, halo 2 and halo 3, respectively. Each row corresponds to one value of the initial gas fraction. From top to bottom these are 0, 20, 50, 75 and 100%. The simulations initially with no gas will have only the DISK as baryonic component and the simulations with initially a purely gaseous disc will have no DISK component. Thus all blocks of figures have missing panels. Fig. 4 gives the face-on views at time $t = 6$ Gyr and Fig. 5 at $t = 10$ Gyr. The full evolution of all simulations in all three components can be seen in our short animations¹.

The basic morphological evolution of the DISK and STARS can be roughly described as follows: A bar forms, surrounded in the strong bar cases by a more or less clear ring structure, of the same extent as the bar, i.e. an inner ring (Buta 1995). It should, however, be kept in mind that these figures do not cover all possible morphologies, since the basic halo and total disc profiles are the same in all cases, and all that changes is the halo shape and the gas fraction.

The gas morphology is reminiscent of what was found in the earlier simulations of Athanassoula (1992b), i.e. considerably different from that of the DISK and STARS; the most striking difference being the absence of a bar in the gas component. In the centre there is a strong concentration of gas, which we will hereafter call the gaseous central mass concentration (CMC). This is surrounded by a large very low density annulus, whose inner and outer radii are a function of the simulation parameters and the time. The extent of this annulus increases with time, as can be seen by comparing Figs. 4 and 5. Surrounding this region, there is the disc of gas, in which there are clear spiral segments, but no clear-cut two armed global spirals.

Looking carefully, one can discern in the very low density annulus two thin stripes of gas, linking the CMC to the gas disc surrounding the very low density annulus. Their location with respect to the bar, as well as their extent, links them to the gas concentrations in the shocks on the leading edges of the bar, found e.g. in the purely hydrodynamical simulations of Athanassoula (1992b). They are of course much less symmetric and less well outlined than in those simulations, but this should be expected since the older simulations were response simulations of an isothermal gas in a rigid model bar galaxy and did not include self-consistency, the physics of the gas, star formation, or feedback. It is, nevertheless, clear that it is the same features in the two cases. We examined these features also in our high resolution simulations, with up to 20 times more gas particles and up to five times more DISK and halo particles. We find that the morphology is similar, although one can discern more

details of the flow, and the gaseous density concentrations along the leading edges of the bar are much clearer delineated.

Turning now to the DISK and STARS components and comparing times $t = 6$ and 10, we see that in the latter time the bar is longer and stronger, as expected due to secular evolution (e.g. A03), and the inner ring is more clearly defined.

Both at $t = 6$ and at $t = 10$ Gyr, there is a clear gradient in bar strength from top left to bottom right in the left and middle block of panels. The strongest bars are found for the spherical halo and no gas, and the strength decreases as we go towards initially more triaxial haloes and larger gas contents. This will be established quantitatively in Sect. 4, but can already be qualitatively seen in Figs. 4 and 5. Also the extent of the low density region in the gas component follows a related trend along the same diagonal. Namely, it is largest for spherical haloes and minimum gas content and decreases as the initial halo triaxiality increases and/or as the initial gas fraction increases.

Another such gradient is linked to the outer extent of the projected surface density in all components. This, however, does not necessarily reflect the concentration of each component, but more its total mass. Indeed, we use the same colour coding for all panels of a given component (and the same for the DISK and the STARS). Thus, the surface density of the DISK will be higher for runs with initially less relative gas, while the surface density of the STARS will be higher for runs with an initially higher relative gas content. This could explain the trends seen in Figs. 4 and 5. Namely the old disc seems most extended for the simulations with no gas and its extent decreases as the initial gas fraction increases. The opposite is true for the gas and the stars formed during the simulation.

Presumably due to the gaseous component and the corresponding CMC mass, we obtained in our simulations morphological features which had not been seen so far in pure N-body simulations. In particular, we note an oval (in some cases near-circular) component of high density in the central part of most of the simulations seen face-on. It is quite clear in both the DISK and the STARS components of simulations with e.g. initially 50% gas and its size is of the order of one third of that of the bar (Figs. 4 and 5). At first sight one could mistake this for a classical bulge. For our simulations, however, it is clear that this can not be true, since, by construction, they have no classical bulge. An alternative would be a pseudo-bulge (as named by Kormendy & Kennicutt 2004) or discy bulge (as named by Athanassoula 2005b). A third alternative interpretation would be to link this component to the barlens, which was discussed recently by Laurikainen et al. (2011) when they studied the central region of many NIRS0S galaxies. This is denoted by *bl* and is generally distinguished from nuclear lenses by its much larger size. Typical examples of a *bl* can be seen in NGC 2983 (figure 8 of Laurikainen et al. 2011) and in NGC 4314 (figure 9 of the same paper, where the fine-structure in the central regions confirms that this component cannot be a bulge). The nature of these components, their formation mechanism, as well as their properties will be discussed elsewhere.

3.4 Morphology of the gaseous CMC at the late simulation times

Fig. 6 gives a detailed view of the central region of two simulations and shows clearly that the gaseous CMC has a rather complex structure. It has a small, high density inner part, which can be clearly seen as a central white feature in this figure. This is elongated roughly along the bar. It forms early on in the evolution and is usually larger at early times than at later ones. Its size and axial ra-

¹ <http://195.221.212.246:4780/dynam/movie/gtr>

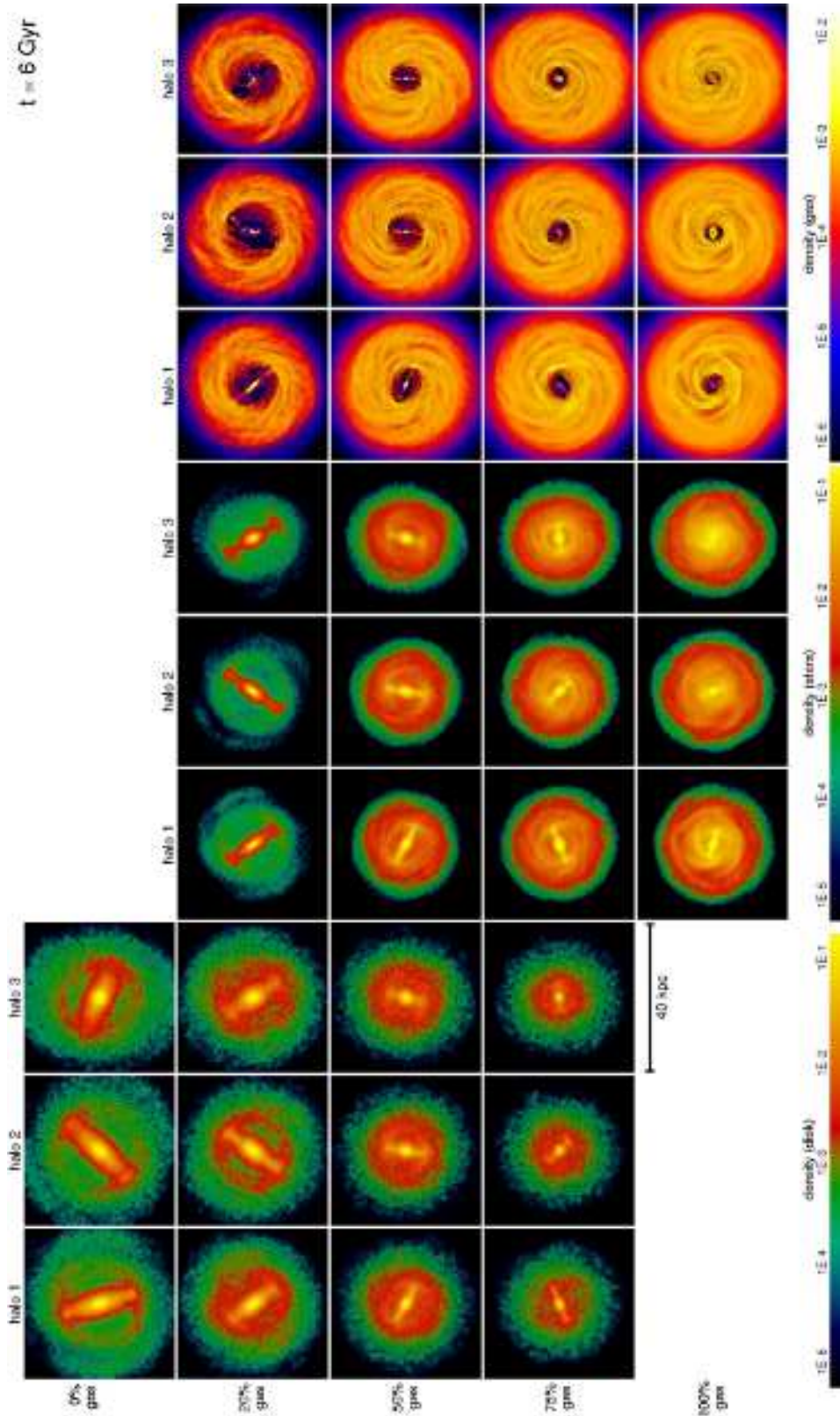


Figure 4. Face-on views of the DISK, STARS and gaseous components of our simulations at $t = 6 \text{ Gyr}$. The first three columns correspond to the disc component (old stars), the next three to the stars that were formed during the simulation and the last three to the gas. The first, fourth and seventh columns show results for simulations with halo 1, the second, fifth and eighth with halo 2, and the third, sixth and ninth to halo 3. Different rows correspond to different initial gas fractions, as indicated in the leftmost part of the figure. Rotation is in the mathematical sense, i.e. counterclockwise. Colour represents projected density and the range is the same for all panels corresponding to the same component and the corresponding numerical values are given by the colour bars in the bottom of the plot. The size of each square box corresponds to 40 Kpc.

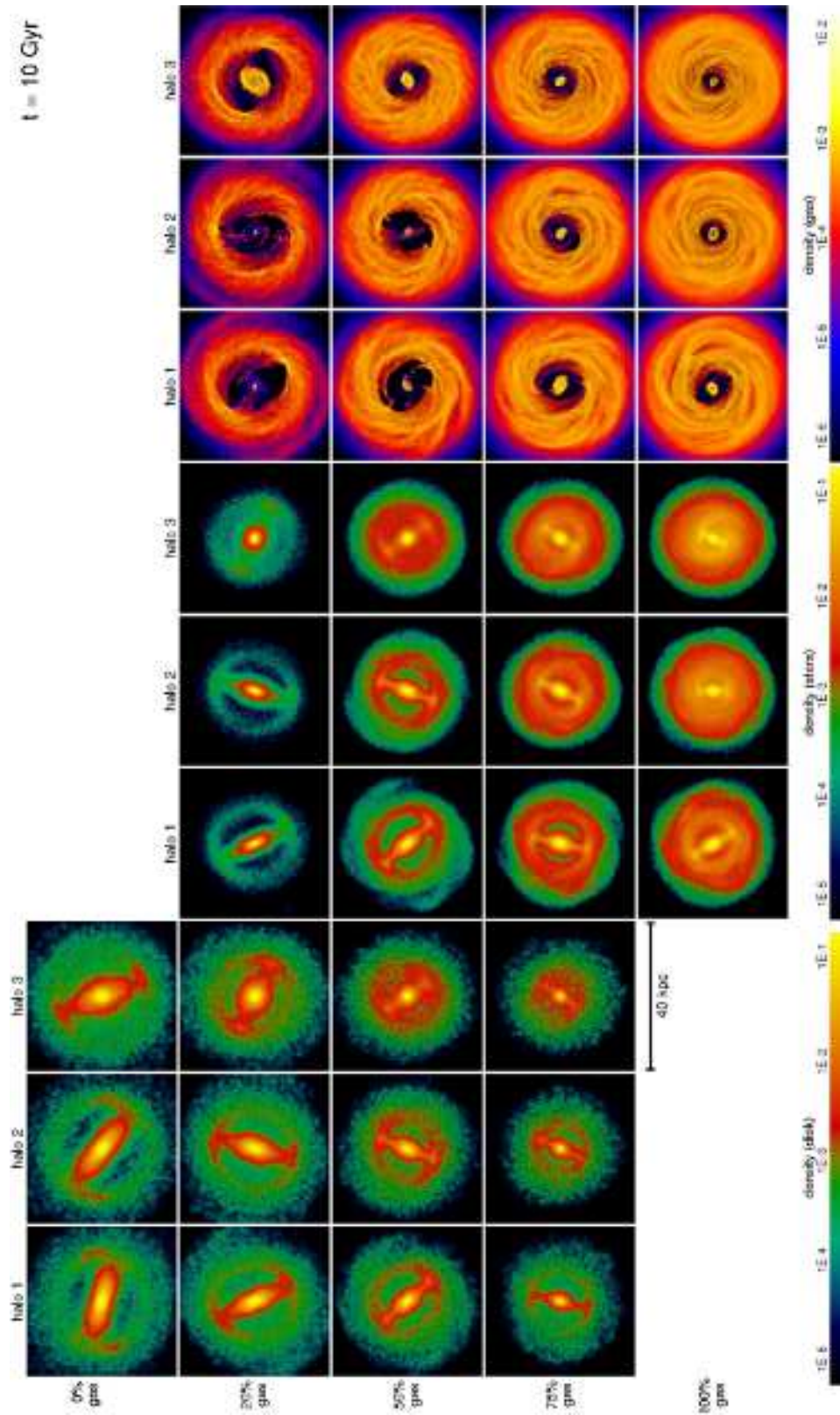


Figure 5. As for Fig. 4, but at $t = 10$ Gyr.

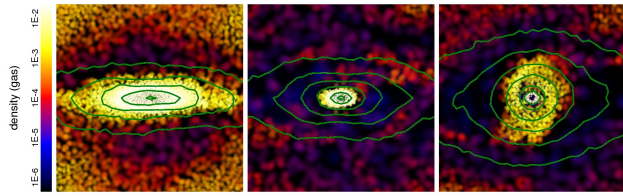


Figure 6. Gas density in the central region of two simulations. The left panel shows simulation 109 at time 2.7 Gyr, the middle one the same simulation at time 5.07 Gyr and the right panel simulation 115 at time 9.04 Gyr. Colour is according to the projected density as given by the colour bar on the left of the panels. The snapshots are rotated so that the bar is horizontal and the size of the boxes is 8×8 kpc. The green lines on all three panels show the isophotes for the combined DISK and STARS components.

tion vary considerably with time. Eye estimates give a representative outline of 0.75 by 0.6 kpc, but at late times it can be considerably smaller, while at early times it can be as large as 1.8 by 0.8 kpc. It is particularly clear in simulations with initially 20%, or 50% gas where it is clearly seen to form first, before the outer component. In the initially 20% cases this component has a rather interesting morphological evolution. It is already present at $t = 2.5 \pm 0.5$ Gyr, where it can be seen as a rather extended component. Its central density is considerably lower than that of its outer part and it can therefore be considered as an elongated inner ring. As it evolves, it becomes smaller and rounder and has almost acquired its final shape and extent by $t = 5 \pm 1$ Gyr. Over some part of the simulation this could therefore be considered as either an inner ring, or an inner gaseous bar, as has been found in previous simulations (Heller, Shlosman & Englmaier 2001).

The gaseous CMC has also a second, considerably more extended component (yellow in Fig. 6). This has lower density and is oriented roughly perpendicular to the bar. Its outline is less well defined than that of the (white) inner component and is more irregular. Its typical size is between 1 and 3 kpc, but in some cases can be even larger. It is not very elongated, with, in many cases, an axial ratio of the order of 2:3. It forms considerably later than the white inner component. In general, it forms earlier for runs with initially strongly triaxial haloes (halo 3) and later in simulations with an initially more spherical halo. There is also a general trend between the initial gas fraction and the time at which this component forms, in the sense that it forms earlier in more gas rich cases. In fact it has not formed by the end of the simulation ($t = 10$ Gyr) for runs 106 and 109 which have initially only 20% gas and spherical or mildly triaxial haloes, respectively, and it forms only after 9 Gyr for runs 111 and 114 which have initially 50% gas and the same haloes.

4 BAR STRENGTH EVOLUTION

The time evolution of the bar strength is shown for all runs in the upper panels of Fig. 7. It was obtained as described in Sect. 2.3 and then smoothed with a Savitzky-Golay filter (Press et al. 1992). We wilfully chose filter values that smooth out not only the noise, but also some relatively high frequency oscillations which we will discuss in detail in Sect. 7, so as to view only the global evolution. The evolution for the various simulations is displayed here so as to show best the effect of the initial gas fraction. Fig. 8 displays the same data as Fig. 7, but now so as to reveal best the effect of halo initial triaxiality. Moreover, in Fig. 8 we used much less smoothing, smoothing out only what we verified by eye is indeed noise. From these two figures it becomes clear that the effect of the initial gas

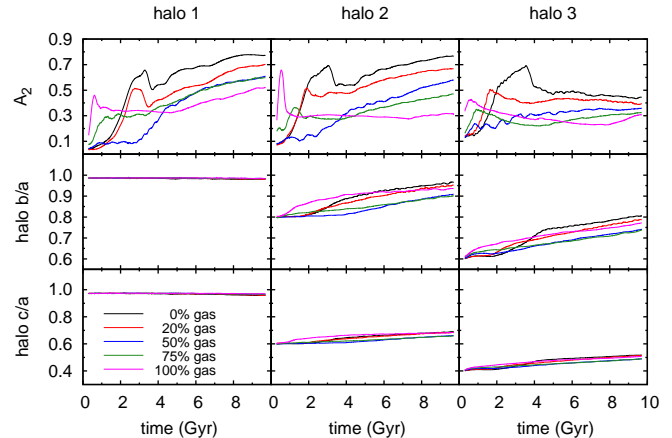


Figure 7. Time evolution of three quantities. From top to bottom the rows of plots give the bar strength (A_2), the halo axial ratio in the equatorial plane (b/a) and the halo flattening (c/a). The three columns correspond to the three different halo models. In the online version, the different initial gas fractions are shown with lines of different colour, namely black for 0%, red for 20%, blue for 50%, green for 75% and magenta for 100% gas, as explained in the panel of the first column and third row. In this display one can easily see the effect of the initial gas fraction on the results.

fraction is very crucial, even more so that the effect of the initial halo triaxiality. Note also that their effect prevails at different times. More specifically we can say the following:

The time at which the bar starts forming depends considerably on the halo triaxiality (Fig. 8) and must be presumably due to the triggering by the halo non-axisymmetry. This effect of triaxiality can be clearly seen in all cases, except those with a strong initial gas fraction where initial disc instabilities in the inner disc parts and the formation of an inner bar do not allow us to distinguish when the main bar starts growing.

All models with no gas and the model with 20% gas and a spherical halo (run 106) have the same *four* evolutionary phases, independent of their halo shape: a fast growth phase, followed by a plateau-like part and then a sharp decrease (see also MA10). The fourth and final phase is that of a slow secular evolution. The maximum values after the growth phase are roughly the same in all gas-less runs and so is the amount of decrease after the plateau, while the times at which these features occur changes little between runs.

The remaining models have fewer evolutionary phases and in many cases it is difficult to distinguish between them. The two simulations with initially 20% gas and a triaxial halo have a similar time evolution of the bar strength, which resembles the one described above, but lacks the plateau right after the phase of the bar growth, while the drop is not as clear-cut. We can thus say that there are three evolutionary phases, first a bar growth to a maximum value, followed by a short decrease phase and finally a slow secular evolution phase.

For all simulations with a strong initial gas fraction (50% or higher) the $m = 2$ strength curves are simpler, and have fewer evolutionary phases. In particular for the cases with initially 50% gas and a spherical, or mildly triaxial halo there is first a time interval during which axisymmetry prevails, followed by a time of bar growth. Both these time intervals are much longer than in the gas-less or gas-poor cases described above, so that we can describe this growth as *secular growth*. This is followed, as in the previously described runs, by a secular evolution phase.

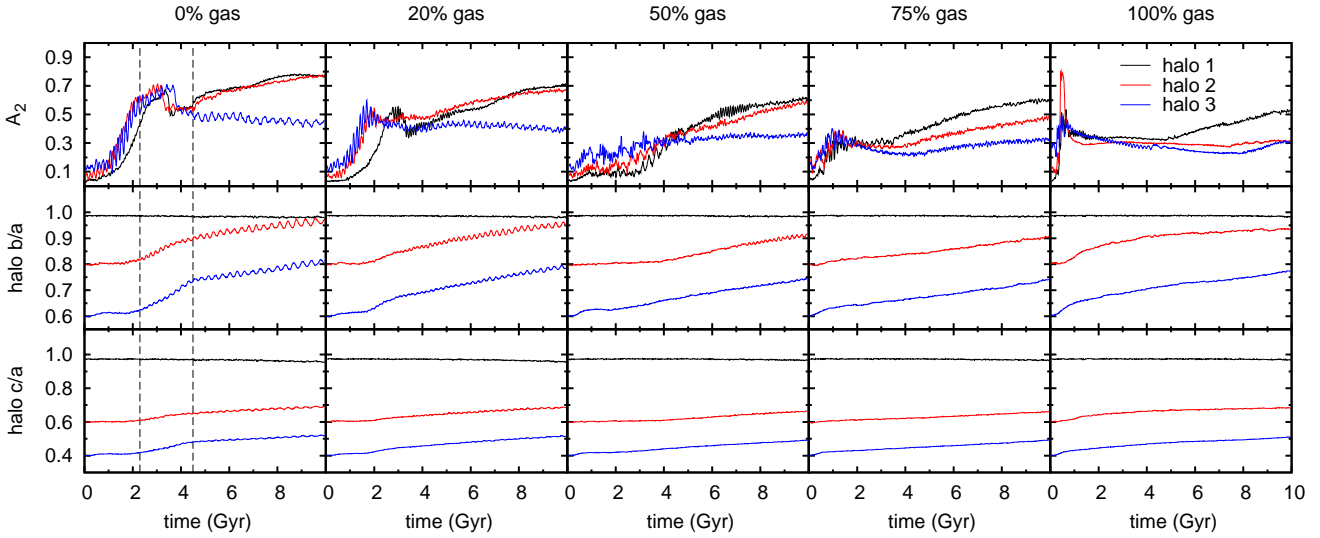


Figure 8. This figure shows the same information as Fig. 7, but now the data is displayed so as to show best the effect of halo triaxiality. From top to bottom the rows of plots give bar strength, the halo axial ratio in the equatorial plane and the halo vertical flattening. The five columns correspond to the five different initial gas fractions and the different haloes are shown with lines of different styles and colour, as given in the upper right panel. The black dashed vertical lines in the first column of panels outline the time range during which the b/a axial ratio displays a strong growth.

Understanding the evolution of gas-rich simulations (initially 75%, or 100% gas) is more complex and we need information on the time evolution of R_{max} , the radius at which the $m = 2$ relative Fourier component is maximum, which we give in Fig. 9. Viewing animations of the evolution of the disc component we see that in the first Gyr or so, several noisy, short-lived, non-axisymmetric features develop in the STARS component which, since these stars are recently formed, is still quite cold (i.e. it has a low velocity dispersion). These features can be spirals, distorted bars, or rings and contribute a lot of noise to the results in Fig. 7 to 9 in the very early times. A particularly strong such feature contributes a very strong and narrow peak of the $m = 2$ strength for run 120 (see Figs. 7 and 8).

As these features subside, a very short bar forms, which we can call an inner bar. The corresponding values of R_{max} are very small (Fig. 9). The main bar starts growing well after the inner bar and, when it becomes sufficiently strong it provokes an abrupt jump of the value of R_{max} to a considerably larger value, compatible with what one would expect for a main bar. Fig. 9 shows clearly that this jump occurs at later times for runs with higher gas fractions and more prolate haloes, in good agreement with the results we presented already for simulations with initially up to 50% gas and with the more qualitative impression one gets from the face-on evolution animations. Thus, in gas-rich cases one has to consider the $A_2(t)$ curves as a result of the growth and evolution of two components combined, one which can be called an inner bar and occurs earlier, before the bar itself has grown, and a second one which is the bar.

All evolutions, for all gas fractions and for all halo types, end with a phase of slow secular evolution, whose duration and strength varies from one simulation to another. In this phase the effect of the halo shape is very strong. In spherical halo cases, and for all initial gas contents, there is strong secular evolution, as witnessed by the slope of the corresponding $A_2(t)$ curves. At the other extreme, halo 3 cases (initially strongly triaxial) have at the best a mild secular evolution (Fig. 8). Halo 2 cases are intermediate, more similar to spherical cases in gas-less or gas-poor cases and more similar to the strongly triaxial cases in gas-rich ones.

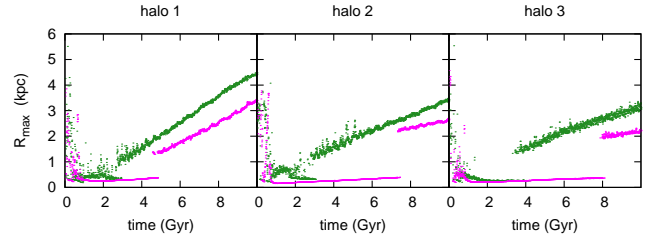


Figure 9. R_{max} , the radius at which the relative $m = 2$ amplitude is maximum, as a function of time. The green points are for a simulation with initially 75% gas and the magenta ones for one with initially 100% gas. From left to right the three panels correspond to halo 1, halo 2 and halo 3, respectively.

There is thus a duality in the effect of the non-axisymmetric forcing of the triaxial halo on bar evolution. In the very early times this forcing can trigger bar formation, so that bars in triaxial haloes grow earlier than in spherical ones, as already discussed in the beginning of this section. On the contrary, at the later stages of evolution, when the bar is well grown, triaxiality hinders bar growth due to the nonlinear interaction between the two non-axisymmetries. Indeed, such an interaction could induce chaos, as advocated by El-Zant & Shlosman (2002). Testing this, however, is not straightforward since one should be careful about eliminating the contribution of ‘confined chaos’ from the statistics, because this can account for galactic structures even for timescales of the order of a few Gyr (see discussion in Athanassoula et al. 2010).

5 ARE BARS LONG-LIVED OR SHORT-LIVED?

5.1 Context

Are bars in isolated galaxies long-lived, or short-lived? A massive central black hole, or a CMC can destroy a bar, provided it is sufficiently massive and/or centrally concentrated (Hasan, Pfenniger, & Norman 1993; Norman et al. 1996). More recent work, however, has shown that the required values are too high

compared to those of observed CMCs (Shen & Sellwood 2004; Athanassoula, Lambert & Dehnen 2005).

The debate became more animated when Bournaud & Combes (2002) reported a number of simulations which included a gas component and in which the bar was destroyed and then formed anew with the help of gas accretion, only to be destroyed again. Three or four such bar episodes occurred during each run. Shen & Sellwood (2004) criticised these simulations for having a time step too long to properly describe the orbits in the central region, so that the bar destruction would be due to an inadequacy of the simulations rather than to a physical effect. In response to this, (Bournaud, Combes, & Semelin 2005, hereafter BCS) decreased the time step of their simulation by a factor of 8 and still found that the bar was destroyed. Using specifically designed simulations, they argue that the effect of the CMC only is indeed not sufficient to fully dissolve the bar. On the other hand, the role of the gas in the angular momentum exchange within the galaxy has a much stronger effect on the bar strength and can indeed destroy it, particularly when it is added to the effect of the CMC. They thus conclude that bars are transient features with a lifetime of 1-2 Gyr.

Debattista et al. (2004, 2006) contributed to this debate by running a number of simulations with either rigid or live haloes and no gas, and, in all but one cases, they witnessed that the buckling instability weakened the bar, but did not destroy it. The exception included gas cooling, but no star formation and no feedback thus resulting in the formation of a particularly massive and compact CMC which destroyed the bar. The Debattista et al. result thus disagrees with the BCS one, because it is the CMC that drives the bar destruction for the simulation of the former and the angular momentum exchange for that of the latter.

Berentzen et al. (2007) also used simulations to examine this issue – including specifically designed ones, like those in BCS – but did not find bar destruction. They argue that what BCS witness is simply the decrease of the bar amplitude due to its buckling. In the Berentzen et al. (2007) simulations (as well as in the later simulations of Villa-Vargas, Shlosman, & Heller 2010) the amplitude of the bar is indeed decreased due to the buckling, but the bar is not destroyed, and after the buckling the bar amplitude starts increasing again.

5.2 Input from our simulations

There are many technical differences between the simulations of the two groups. Bournaud, Combes, & Semelin (2005) have a large number of gas particles (10^6), model the gas with sticky particles and use a rigid halo. The latter may have particularly important consequences, because, as shown by Athanassoula (2002), a rigid halo can not take part in the angular momentum redistribution and thus can not help the bar grow. On the hand, Berentzen et al. (2007); Villa-Vargas, Shlosman, & Heller (2010) have a live halo and an SPH gas description, but the number of gas particles in their simulations is rather low, 40 000 only, and they do not undergo any star formation, feedback or cooling.

The simulations we describe in this paper can be used to shed new light on this important and not yet settled issue. Our simulations have a large number of gas particles (Sect. 2.1) and we have also looked at the bar strength evolution in the three simulations with a yet higher number of particles (up to 4 million gas particles). Furthermore, all our simulations have a live halo with a sufficient number of particles to describe the resonances adequately (Athanassoula 2002) and their softening is 50 pc, thus ensuring

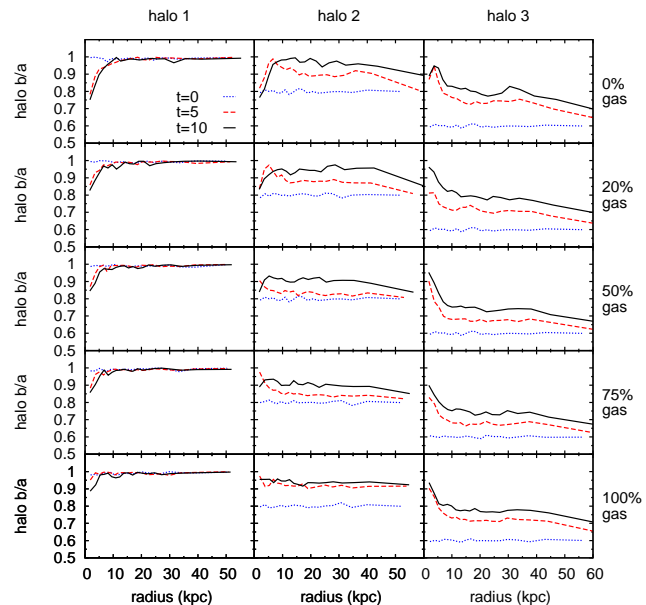


Figure 10. Radial profile of the halo equatorial axial ratio (b/a) for three times during the simulation ($t = 0, 5$ and 10 Gyr) and for all simulations. The layout is as for Fig. 1

a high spatial resolution. All previous simulations concerning bar longevity were performed with spherical haloes, so for comparisons we will restrict ourselves to our simulations with spherical haloes. Both the animations of these simulations and the plots of the bar strength time evolution (Figs. 7 and 8) show clearly that for the spherical halo cases the bar is never destroyed, and this for all gas fractions. The drop of the $m = 2$ amplitude observed at very early times in simulations whose disc is initially all gas, or very gas rich (Fig. 7 and 8) is due to the demise of initial gas instabilities which are reflected in the STARS component. As already discussed in Sect. 4, these occur in the inner parts of the disc. Thus one can not exclude the dissolution of inner bars with a length of the order of, or considerably less than 1 kpc.

We thus conclude that our simulations argue against bar destruction and agree with those of Debattista et al. (2004, 2006); Berentzen et al. (2007) and Villa-Vargas, Shlosman, & Heller (2010), even though the halo radial profiles and the way the gas is modelled varied strongly from one set of simulations to another.

We can, furthermore extend this discussion to triaxial haloes. Fig. 7 shows that, even in simulations with a triaxial halo, the bar does not get destroyed, although its $m = 2$ amplitude in the case with initially 100% gas starts and stays small. In some of the simulations with an initially strongly triaxial case (halo 3), however, the $m = 2$ amplitude shows a very small decrease with time. As can be seen by comparing Figs. 4 and 5 this is not due to a weakening of the bar, but to the growth of the barless component (Sect. 3.3). Furthermore, this weakening is slow that it would have a sizeable effect only at times much longer than the a Hubble time.

6 HALO PROPERTIES

6.1 Radial profiles of halo equatorial axial ratios

Fig. 10 shows the radial profile of the halo equatorial axial ratio (b/a) for three times ($t = 0, 5$ and 10 Gyr) and for all

simulations. In simulations with an initially spherical halo (halo 1) and no gas, the innermost part becomes during the evolution considerably triaxial, thus forming a bar in the halo component. This structure was already spotted in a number of simulations (e.g. Debattista & Sellwood 2000; O’Neill & Dubinski 2003; Holley-Bockelmann et al. 2005; Berentzen & Shlosman 2006) and its properties have been studied in some detail in Hernquist & Weinberg (1992), Athanassoula (2005b, 2007) and Colín et al. (2006). It is called ‘halo bar’ or ‘dark bar’ and is considerably shorter than the disc bar, rotates with roughly the same angular velocity and is due to the angular momentum exchange between the near-resonant particles in the inner halo and the near-resonant particles in the disc bar region (Athanassoula 2007, A03).

This feature is also seen in all our simulations with a spherical halo and its amplitude depends on the gas fraction, being the strongest in gas-less simulations. It is also seen in cases with a mildly triaxial halo (halo 2) and with an initial gas fraction up to $\sim 50\%$ and, albeit it to a much lower extent, in the simulation with the strongly triaxial halo (halo 3) and no initial gas. The other simulations do not have this feature and, on the contrary, show an increase of b/a at small radii. The initial gas fraction that limits the simulations with a halo bar from those with a rounder centre depends on the halo shape and is in fact between 50 and 75% for the initially less triaxial halo and around 0% for the strongly triaxial one. It is clear that the existence of this feature is linked with the existence of a strong bar in the disc component, since the snapshots that do not have it either have no bar, or a only a very weak one. We find a rough limit of $A_2 > 0.5$ for the halo bar to exist.

There is also a rather abrupt drop of b/a in the outermost parts of the halo. Although the halo is indeed less spherical in its outermost parts, the abruptness of the transition is an artefact due to the way the b/a values were obtained. Indeed as discussed in Section 2.3, in order to calculate the inertial tensor the particles were binned by their local density value in bins of equal number of particles and, since the density drops considerably with radius, the radial extent of the outer bin is much larger than that of the others.

Barring this drop of b/a in the innermost and the outermost parts, globally the halo evolves towards axisymmetry. This time evolution can be better seen in the second row of panels in Figs. 7 and 8 and is discussed in Sect. 6.2.

6.2 Time evolution of the halo axial ratios

Fig. 7 shows the time evolution of b/a , the halo axial ratio in the equatorial plane, (middle panels) and c/a , the halo flattening (lower panels). The data are displayed so that they show best the effect of initial gas fraction.

Changes of the axial ratios in the spherical haloes are very small, of the order of a few per cent over 10 Gyr. They show very little dependence on the gas fraction. This small gradual flattening, i.e. small decrease of the c/a ratio with time, is not due to the simulation starting somewhat off equilibrium. This would have led to a fast rearrangement and not a gradual, slow evolution. Also many tests have shown us that the iterative method we use (Rodionov et al. 2009; Rodionov & Athanassoula 2011) can produce initial conditions very near equilibrium for times sufficiently long for us to be able to follow bar formation uninhibited by other instabilities due to the inadequacy of the initial conditions. Nevertheless, the evolution of the galaxy due to the formation and evolution of the bar will influence the halo and can well account for the small changes we see in its axial ratios.

On the other hand, simulations with an initially triaxial halo,

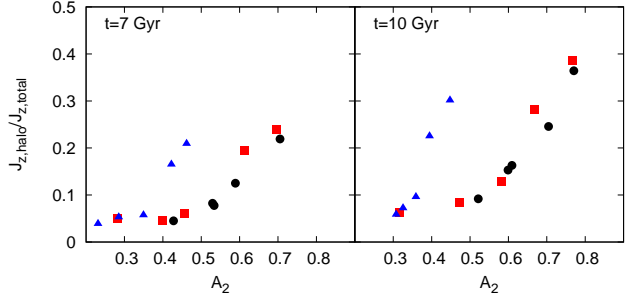


Figure 11. Correlation between the fraction of angular angular momentum absorbed by the halo and the bar strength. Symbols represent different halo shapes: filled circles (black online) for halo 1, filled squares (red online) for halo 2 and filled triangles (blue online) for halo 3.

have a much stronger time evolution of their b/a and c/a values than simulations with initially spherical halo, as expected. In simulations with no gas and with an initially triaxial halo we confirm that the halo becomes considerably less triaxial during the evolution, as already found by Berentzen & Shlosman (2006), Heller, Shlosman, & Athanassoula (2007b) and MA10. Our results allow us to extend this conclusion to simulations with gas. The corresponding haloes also become more spherical during the evolution, but the effect is smaller than for the gas-less models. Nevertheless, a systematic dependence on the gas fractions is inconclusive, as for example in the middle right panel of Fig. 7 (halo 3) the initially 100% and 20% gas end up with roughly the same b/a ratio, which is larger than that of the 50% and 70% gas cases. The changes in b/a are accompanied by a change in c/a , which is nevertheless much smaller than the b/a change. Both together bring the haloes nearer to sphericity. Also the amount of gas has less effect on the change of the c/a than on that of the b/a .

The middle and lower panels of Fig. 8 display the same data, but so as to show best the effect of the halo. The b/a for halo 2 starts from 0.8 and ends roughly in the range 0.9 to 0.98, while for halo 3 it starts from 0.6 and ends roughly in the range 0.75 to 0.8. The corresponding numbers for c/a are from 0.6 to 0.65/0.7 for halo 2, and from 0.4 to 0.5 for halo 3.

This way of plotting the data also allows us also to see best the imprints of the various phases of bar formation and evolution on the temporal evolution of the b/a and c/a profiles. For simulations where the bar growth has four phases (see Sect. 4), the b/a growth has clearly three phases. A first phase where the b/a value hardly changes, a second phase with a strong growth and finally a third phase with a weaker secular growth. To make this yet clearer, we added on Fig. 8 vertical lines roughly delineating these three phases for the 0% gas case. By extending them to the upper panel (A_2 as a function of time) we see that the first phase corresponds to the bar growth phase, the third one to the bar secular evolution phase, and the intermediate phase encompasses the flat A_2 phase, the abrupt fall of A_2 and the very first steps of the bar secular evolution. The three phases in the b/a evolution are clearly seen only in those runs where the A_2 has four phases (see Sect. 4). Short duration strong growths are also seen in other cases and are again linked to specific $m = 2$ phases. For example in initially 100% gas cases there is a strong b/a growth roughly in the first Gyr, i.e. the time when the strong $m = 2$ features appear. Thus the b/a growth is clearly linked to the bar formation and evolution, as already proposed in MA10.

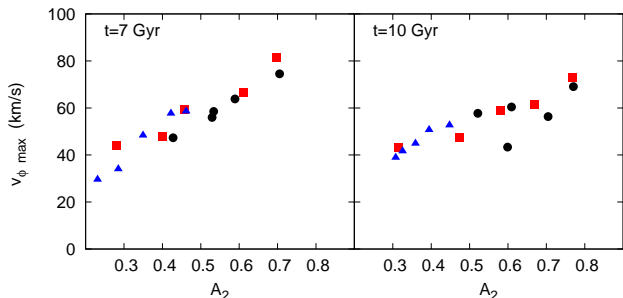


Figure 12. Correlation between the peak tangential velocities of the halo permanently disc-like particles (see text) and bar strengths. Symbols represent different halo shapes: filled circles (black online) for halo 1, filled squares (red online) for halo 2 and filled triangles (blue online) for halo 3.

6.3 Angular momentum redistribution

Previous N-body simulations have shown that barred galaxies evolve by redistributing their angular momentum and that haloes play a substantial role in this redistribution by absorbing angular momentum at their various resonances, mainly the inner Lindblad resonance, the corotation resonance and the outer Lindblad resonance (Athanasoula 2002). Furthermore the fraction of the initial angular momentum that is absorbed by the halo correlates well with the bar strength (A_{03}).

Here we extend this to simulations with gas and/or with triaxial haloes. The results are given in Fig. 11 for $t = 7$ (left panel) and 10 Gyr (right panel). We note that simulations with an initially spherical halo (halo 1) share the same trend as those with an initially mildly triaxial halo (halo 2), while simulations with an initially strongly triaxial halo (halo 3) have considerably higher halo angular momentum exchange, at least for the two cases with the strongest bars. This must be linked to the extra torque due to the triaxial halo, but its study is beyond the scope of this paper. The Pearson correlation coefficient (Press et al. 1992) for the simulations with halo 1 or halo 2, taken together, is 0.89 (0.90) and for those with halo 3 it is 0.93 (0.97) for time 7 (10) Gyr.

6.4 Halo kinematics

The angular momentum redistribution within the galaxy brings significant changes to the halo velocity distributions (Athanasoula 2005a, 2007; Colín et al. 2006). Halo particles located relatively near the disc equatorial plane acquire tangential velocity and rotate in the same sense as disc particles, albeit much slower (Athanasoula 2007). This result was extended to initially non-spherical haloes by MA10. We will here examine how the presence of gas can influence these results.

We follow Athanasoula (2007) and select all particles that remain near the equatorial plane for a considerable time interval and call them ‘disc-like’ for brevity. In practice, we choose particles for which $|z| < 2$ kpc for all times within the range $7 < t < 10$ Gyr (for $t = 10$ Gyr) and $4 < t < 7$ Gyr (for $t = 7$ Gyr). The resulting velocity radial profiles of these particles are very similar to those shown in Fig. 11 of Athanasoula (2007), or Fig. 23 of MA10 and we thus do not display them here. They show that mean tangential velocity curves for such ‘disc-like’ halo particles can reach velocities of the order of 80 km/sec. They also show that this rotation is fastest for the spherical model with no gas, which has the strongest bar, and slowest for the model with initially the most gas and most triaxial halo, i.e. follows a trend similar to that of the bar strength.

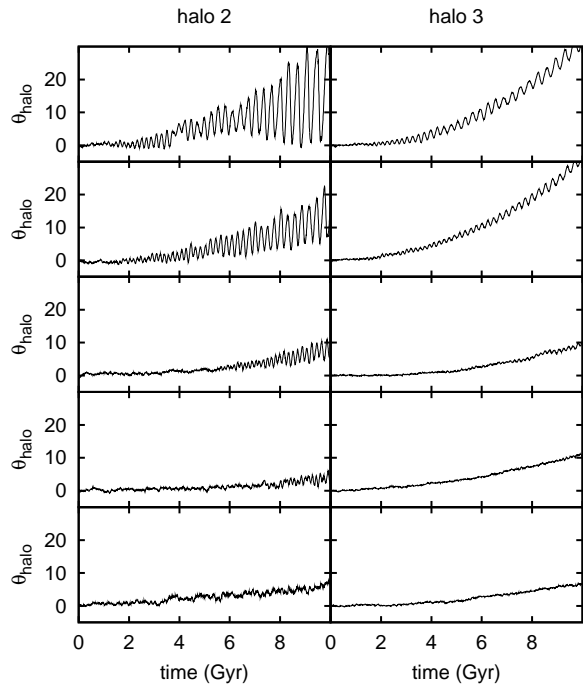


Figure 13. The angle of the halo major axis as a function of time for the 10 simulations with non-axisymmetric haloes. The left (right) column displays information on simulations with initially mildly (strongly) triaxial haloes. From top to bottom the initial gas fraction is 0%, 20%, 50%, 75% and 100%.

In order to illustrate this trend, we plot in Fig. 12 the peak tangential velocities of the ‘disc-like’ halo particles versus the disc bar strengths of the corresponding model for $t = 7$ and $t = 10$ Gyr. It is clear that models with stronger bars have higher peak rotation. In fact, the corresponding correlations are quite strong, with Pearson correlation coefficients (Press et al. 1992) of 0.95 and 0.86, for $t = 7$ and 10 Gyr, respectively. This clearly links the origin of these tangential velocities to the bar and is in good agreement with results of Athanasoula (2007) and MA10.

In Fig. 12, contrary to the results in Fig. 11, the simulations with an initially strongly non-axisymmetric halo (halo 3) lie on the same correlation as those of halo 1 and halo 2. This argues that there is not a one to one correspondence between the halo population that absorbs the angular momentum and the population with the largest v_ϕ . Indeed in the latter there are many particles that already initially were considerably rotating. An in depth analysis of the orbital structure in the halo and its evolution as angular momentum is absorbed will be given elsewhere.

6.5 Halo bulk rotation

Triaxial haloes are not simple geometrical objects. As discussed in Sect. 6.2, the inner part presents an elongation, which we called halo bar and which is rotating together with the bar in the disc. Further out also the halo is non-axisymmetric, but this non-axisymmetry is a remnant of the initial, non-rotating triaxiality and is not due to the bar. We measured the angle of the main halo part using the region with $10 > r > 30$ kpc, thus avoiding the halo bar and the region outside it, where it is not easy to disentangle the halo bar from the outer triaxiality, as well as the outermost region where the density is low and which interacts little with the disc compo-

ment. We proceeded as discussed in Sect. 2.3 and plot the angle of the halo major axis in Fig. 13.

We note that in all cases the haloes acquire some bulk rotation, even though the initial halo was built in equilibrium as non-rotating. In general, we find larger rotations for initially strongly non-axisymmetric haloes and for low initial gas fractions. From Fig. 11 we see that in these cases more angular momentum is given to the halo. It is therefore reasonable to assume that part of the angular momentum absorbed by the halo is taken by the bulk rotation and part by the motion of the individual ‘disc-like’ halo particles (see Sect. 6.4). In good agreement with this assumption, the halo rotates anticlockwise, i.e. in the direct sense.

We also note from Fig. 13 that the angle of the halo major axis also displays some short period oscillations which we will discuss further in Sect. 7. Mentally ignoring them, we see that the halo bulk rotation increases considerably with time, contrary to the bar pattern speed, which has been shown to decrease with time (e.g. Debattista & Sellwood 2000, A03, Berentzen et al. 2007).

Fig. 13 also shows that the halo bulk rotation is very small, of the order of $5^\circ - 30^\circ$ over a period of 10 Gyr, i.e. even slower than what was found by Bailin & Steinmetz (2004), Heller, Shlosman, & Athanassoula (2007b) and MA10, where the halo was found to rotate about 90° in a Hubble time. The difference, however, is smaller if one takes into account the increase of the halo bulk rotation with time and compares only the later times.

7 INTERACTION BETWEEN THE VARIOUS NON-AXISYMMETRIC COMPONENTS

In a simple barred galaxy, the bar is the only non-axisymmetric component and its building blocks are periodic orbits elongated along the bar (Contopoulos & Papayannopoulos 1980; Athanassoula et al. 1983). In the case of a galaxy with two bars, an outer main bar and an inner small one, the basic building blocks are loops, i.e. one-dimensional closed curves such that particles along them at a given time return to the same curve (as viewed in the frame co-rotating with one of the bars) after the two bars return to the same relative position (Maciejewski & Sparke 1997). It is intuitive that, in such cases, the two bars can not rotate rigidly through each other, but should show oscillations with the relative frequency of the two bars. This can indeed be shown using the loop concept. Figure 2 in Maciejewski & Sparke (2000) and figure 6 in Maciejewski & Athanassoula (2007) show that a loop corresponding to an inner bar is more elongated when the two bars are perpendicular to each other and less elongated when the two bars are aligned.

Double bars and the associated oscillations were also witnessed in a number of simulations (e.g. Rautiainen et al. 2002; Heller, Shlosman, & Athanassoula 2007a, and references below and therein). There is a general agreement that the oscillation frequency is equal to the relative frequency of the two bars, but considerable disagreement concerning the remaining results. The simulations of Heller, Shlosman & Englmaier (2001) showed the formation of an inner ring/bar component which is more elongated when it is parallel to the main bar, contrary to the loop predictions. A similar behaviour was found for the double bar systems of Heller, Shlosman, & Athanassoula (2007b). Both these works included gas in the simulations. On the other hand, Debattista & Shen (2007) found that the strength of the outer bar has a maximum when the two bars are aligned and a minimum when the two bars are perpendicular to each other. The strength of the inner bar

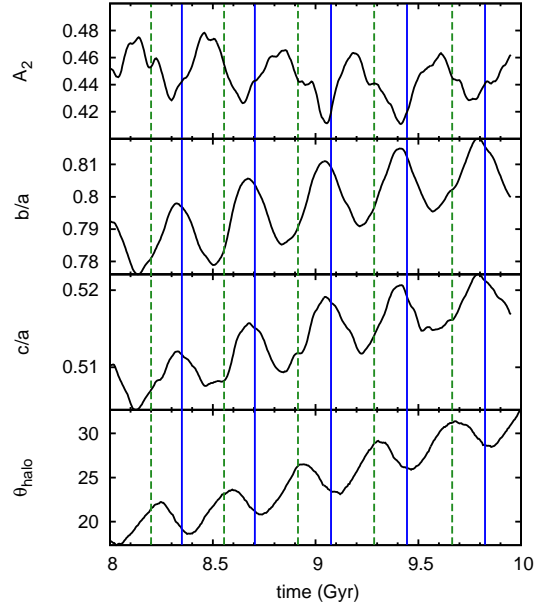


Figure 14. Bar strength (upper panel), halo b/a (second panel) and c/a (third panel) axial ratios and angle of the halo major axis (θ_{halo}), all as a function of time for a run with 0% gas and an initially strongly triaxial halo (halo 3). The scales and the time range were chosen so as to show best the oscillations. Vertical solid lines (blue in the online version) correspond to times when the directions of the halo and the bar major axes are aligned, while dashed lines (green in the online version) correspond to the times when they are perpendicular.

is maximum when the two bars are perpendicular and minimum when they are aligned, in good agreement with the loop results (Maciejewski & Sparke 2000; Maciejewski & Athanassoula 2007) and the simulations of Rautiainen et al. (2002). However these simulations and loop calculations do not include gas. It is thus of interest to revisit this question with our simulations.

Figs. 14 and 15 show, for two different simulations, the oscillations with time of the bar strength, of the halo axial ratios b/a and c/a , and of the angles of the halo and gas CMC major axes. The b/a and c/a were calculated from the region with $10 > r > 30$ kpc, for the reasons discussed in Sect. 6.5. We also indicated by vertical lines in both figures the times at which the bar and the halo major axes are parallel, or perpendicular. Note that, to zeroth order approximation, when the bar and halo major axes are aligned, the A_2 has a minimum and the b/a has a maximum, i.e. both are nearer to axisymmetry at that time. On the contrary, when the bar and halo major axes are perpendicular, the A_2 has a maximum and the b/a has a minimum, i.e. both are further away from axisymmetry at that time. The period of these oscillations is compatible with the relative frequency of the bar and halo rotation. Note also that the c/a and the angles of the halo and gaseous CMC major axes also have oscillations at the same frequency. Those of c/a are in phase with respect to the oscillations of b/a , while those of the halo and gaseous CMC major axes are at a maximum when those of b/a are at a minimum. In as much as comparisons are possible, the above results are in agreement with those of the loop theory.

Note, however, that this description is only a zeroth order approximation of the simulation results, since in fact the quantities whose time evolution we follow display patterns which are more complex than single oscillations with a constant frequency. This is due to the self-consistency and the strong non-linearity present in the simulations, which leads to results more complex than the sim-

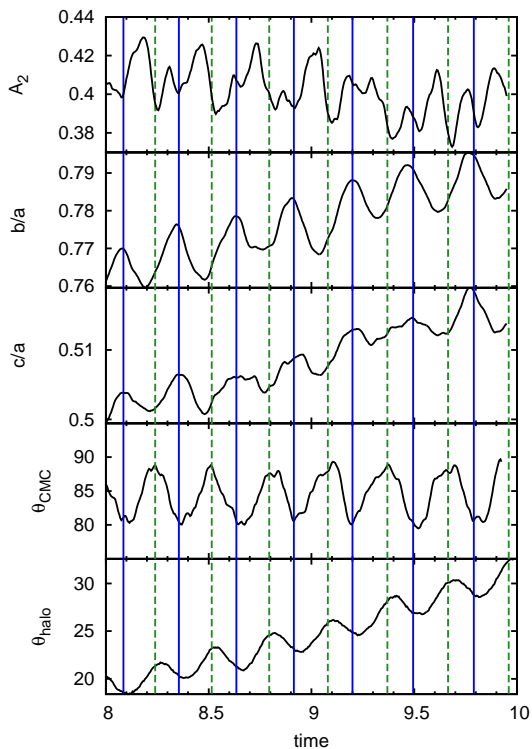


Figure 15. Time evolution of the bar strength (upper panel), the halo b/a and c/a axial ratios (second and third panels from the top), the angle between the major axes of the gaseous CMC and the bar (fourth panel from the top) and the angle for the halo major axis (lowest panel), for a simulation with initially 20% gas and a strongly triaxial halo (halo 3). The scales and the time range displayed are such so as to show best the oscillations. Solid lines (blue in the online version) correspond to times when the directions of the halo and the bar major axes are aligned, while the dashed lines (green in the online version) correspond to the times when they are perpendicular.

ple models with rigid components and constant pattern speeds can describe. For example, the halo can not be described as a single rotating ellipsoid because the elongation in its inner parts follows the bar while the elongation of its outer parts hardly rotates. More precisely, we should talk about two groups of such components. On the one hand there is the triaxial halo, which rotates with a very small angular velocity. On the other hand the main bar, the halo bar and the gaseous and stellar CMCs, which are non-axisymmetric components that rotate with the bar pattern speed. Nevertheless, it is very gratifying that at zeroth order approximations (i.e. as far as the simplifications inherit in the loop theory can permit) there is no disagreement with known theoretical results.

The amplitude of these oscillations varies from one case to another. It increases with increasing bar strength and also with increasing halo triaxiality, as could be expected since strongest interactions are expected when the two interacting non-axisymmetries are strongest.

8 FURTHER DISCUSSION

8.1 Advantages and limitations of this work

Our simulations are dynamical rather than cosmological, i.e. they are set so as to allow us to study best a given effect, in our case the effect of gas and of non-axisymmetric haloes on the growth, evolution and properties of the bar. Thus, as in all dynamical sim-

ulations, the initial conditions are what is sometimes referred to as idealised, i.e. the disc is assumed to have formed first and simulations are started in the time interval after the disc has formed and before the bar starts. This provides optimum conditions for studies of bar formation and evolution.

Compared to previous dynamical simulations, the ones presented here have a number of strong points. The halo is live and is represented by one million particles, a number which, for the adopted halo radial density profile, is sufficient for an adequate description of the resonances and therefore of the angular momentum exchange, thus not biasing the whole evolution (Athanasoula 2002, A03). We have also used a large number of gas particles, in all our standard cases with a mass of $m_{gas} = 5 \times 10^4 M_{\odot}$ per particle. We ran also simulations with a much higher number of gas particles, with a resolution up to $m_{gas} = 2.5 \times 10^3 M_{\odot}$, and made sure there were no qualitative, or important quantitative differences. We, furthermore, have a high spatial resolution with a gravitational softening of 50 pc.

Contrary to most previous dynamical studies of bar formation and evolution, our gas has both a cold and a hot phase and is modelled including star formation, feedback and cooling. We do not claim that our recipes are perfect representations of the interstellar medium. Indeed such perfect recipes are not available (Scannapieco et al. 2012). But they are realistic, certainly much more so than a complete neglect of star formation, which leads to a gas fraction which does not decrease with time. The latter would entail too low a gas fraction during the bar formation and early evolution stages and/or a too high fraction during the secular evolution phase. A more in depth description of the effect of various star formation, feedback and cooling recipes on bar formation and evolution will be given elsewhere.

We put considerable effort so that the initial conditions we generate are as close to equilibrium as possible (Rodionov et al. 2009; Rodionov & Athanasoula 2011), so as to make sure that there are no transients due to inadequacies. This allowed us, for example, to get information on how long the disc can stay axisymmetric before forming the bar, or to measure the bar growth rate.

We made, whenever possible, comparisons between our results and those of previous studies. In most cases, however, it was not possible to make any quantitative comparisons, because in our simulations the gas fraction varies with time, due to the star formation, while in simulations with no star formation it stays constant. It is thus unclear to what (constant) gas fraction value we should be comparing our results to. Indeed, gas fraction can have different effects on the different phases of the bar formation and evolution.

As limitations of this work we can say that we have considered only one mass model and only one set of star formation, feedback and cooling recipes. Furthermore, we have not included modules for chemical evolution, or for accretion, which would have allowed us to follow jointly the chemical and the dynamical evolution, nor have we discussed star formation, stellar populations and chemical abundances. These will be considered in future work.

8.2 The effect of gas on bar growth and evolution

It is clear from the previous sections that gas has a strong influence on bar growth and evolution. Yet the relation is rather complex. Indeed there are a number of effects, sometimes opposing each other.

i) It is known that cold components respond more strongly to any forcing than hot ones (Binney & Tremaine 2008). Since gas is very cold and the stars born from it are much colder than the old

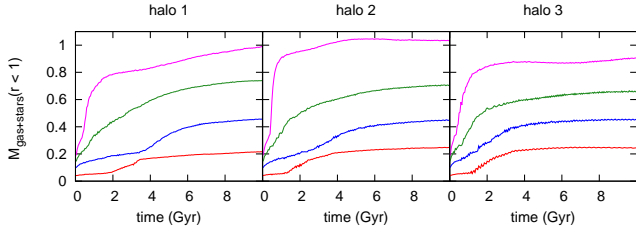


Figure 16. Time evolution of the mass in the central region. We plot here the mass of the gaseous component and of the stars born from it, measured within the central 1 kpc in units of $10^{10} M_{\odot}$. The three columns correspond to the three different halo models. From left to right these are initially spherical, mildly triaxial and strongly triaxial. In the online version, the different initial gas fractions are shown with lines of different colour, namely red for 20%, blue for 50%, green for 75% and magenta for 100% gas.

stars, one could expect that stronger bars would be formed in more gas-rich cases.

ii) The gas also takes part in the angular momentum redistribution within the galaxy. For gas-less simulations, frequency analysis of the orbits has shown that angular momentum is emitted from stars at (near-)resonance in the bar region and absorbed by (near-)resonant material in the halo and in the outer disc. Thus the angular momentum of the disc decreases with time and that of the halo increases by an equal amount. If there is also a bulge, then it also can absorb angular momentum. The above results were first found and tested in simulations by Athanassoula (2002; 2003 and unpublished), and then confirmed by a number of other simulations, with different models and methods (e.g. Martinez-Valpuesta et al. 2006; Ceverino & Klypin 2007; Dubinski et al. 2009; Wozniak & Michel-Dansac 2009; Saha, Martinez-Valpuesta & Gerhard 2012).

Although frequency analyses, as the ones mentioned above, have not been yet performed for simulations including gas, both results from several previous papers (e.g. Berentzen et al. 2004; Bournaud, Combes, & Semelin 2005; Berentzen et al. 2007) and from our simulations argue that gas gives angular momentum to the bar and thus hinders its growth. Thus the bar strength should decrease as the amount of gas increases.

iii) As already discussed in Sect. 5.1, both orbital structure theory and N-body simulations have shown that the existence of a massive and compact CMC can weaken the bar strength. Contrary to some previous studies, in our simulations such a CMC is not put in “by hand”, it results from the evolution (Sect. 3.4). Indeed, the bar pushes the gas inwards where it forms a CMC. In Fig. 16 we plot the mass of the gas and of the STARS in the inner one kpc as a function of time. It shows that in gas-poor simulations the CMC is considerably less massive than in the gas-rich ones. Thus, the CMC will weaken the bar more in gas-rich simulations.

iv) Stars are born in a very thin disc, which gradually thickens with time. The effect of the disc thickness on the bar strength and pattern speed was studied by Klypin et al. (2009). They find that thinner discs host shorter and weaker bars than thicker ones. Applying straightforwardly their result to our simulations we can imply that simulations with less old stars and more gas and young stars will have a larger fraction of their mass in a thin component, and therefore will give rise to bars which are shorter and weaker than those which form in more gas-poor discs.

We have thus listed four ways in which gas can influence the length and strength of bars. Of these, three argue that more gas-rich galaxies will form weaker bars, while one – perhaps the least convincing one – argues for the opposite. In our simulations it is

clear that bars in gas-rich simulations are indeed weaker, arguing that the combined effect of the angular momentum redistribution, of the CMC and of the vertical gas thickness dominates.

8.3 The structure of the CMC

8.3.1 The mass of the CMC as a function of gas fraction

Fig. 16 shows that the CMC mass included within one kpc from the centre increases considerably with the gas fraction, and that this holds for all the halo shapes we considered here. Interpreting this is relatively complex, because there are three competing effects.

i) The first has to do with the total amount of gas in the simulation, since in cases where this is very large, more gas will be pushed inwards, all other quantities staying equal.

ii) On the other hand, runs with a large gas fraction have weaker bars (Sect. 3.3 and 4), so, all other quantities staying the same, less gas is pushed inwards.

iii) A third, most important effect is that the extent (both in radius and in energy range) of the x_2 orbits diminishes as the bar strength increases (Athanassoula 1992a). Therefore, and seen the morphological results in Sect. 3.3, one expects that the x_2 is stronger in cases with more gas.

Our results show that the first and third effects coupled together are stronger than the second one, so that the CMC component is more massive in simulations with more gas and less massive in simulations with less gas.

8.3.2 The existence of both an inner and an outer Lindblad resonance

In Sect. 3.4 we showed that the gaseous CMC has two distinct components. The first one, which we call the inner CMC, has a very small extent and a very high density and it is elongated roughly along the bar. The second one, which we call the outer CMC, has a considerably larger extent, a lower (but still high) density and it is elongated roughly perpendicular to the bar. The two together form the gaseous CMC.

To understand better these structures we froze the potential for a number of simulations and times and calculated in each of those cases a large number of orbits, using as initial conditions the positions and velocities of simulation particles describing the gas, or the very young stars, so as to follow the families of periodic orbits (Sanders & Huntley 1976; Athanassoula 1992a,b). We followed them for 0.5 Gyr each, i.e. sufficiently so as to clearly get the orbital shape. Amongst these orbits, we can divide the regular-looking ones into three categories:

i) Orbits aligned roughly along the bar whose extent is of the order of the bar length, or a sizeable fraction of it;

ii) orbits aligned roughly along the bar but whose extent is very much shorter than the bar, namely of the order of the inner CMC or even less;

iii) and orbits aligned roughly perpendicular to the bar and whose extent is of the order of the outer CMC size or even less.

Orbital structure theory has shown (e.g. Contopoulos 1980) that the orientation of the 2:1 periodic orbits, in simple rigid potentials with an axisymmetric and an $m = 2$ part, changes by 90° at each resonance. More specifically, it is parallel to the bar within the inner ILR (x_1 family), perpendicular to it between the inner and the outer ILRs (x_2 and x_3 families) and again parallel to it between the outer ILR and the CR (x_1 family). Our orbital calculations confirm

this for our more complex potentials and thus explain the formation of the double CMC that we find.

Note that such a CMC morphology can not be seen in the old stars. This can be easily understood, because the velocity dispersion of old stars is much larger than that of young stars (e.g. Nordström et al. 2004). Since the surface occupied by the x_2 family on a surface of section is much smaller for larger energy values, it is much easier for gas and very young stars to be trapped by the x_2 family than for old stars. A fuller discussion of this has been given by Patsis & Athanassoula (2000).

It should be stressed that the existence of two ILRs, the inner and the outer, hinges on the potential having an inner core and can never be found in potentials with a strong cusp. On the other hand, not any potential with a core will have the gaseous CMC morphology that we discussed here, since this depends on the size of the core and the strength of the bar. These will also influence very considerably the values of the sizes and size ratios for both components, since they influence the extent and strength of the x_2 family.

This interpretation of the CMC structure makes a clear prediction. Indeed, orbital structure theory shows that the maximum extent of the x_2 orbits is smaller than or of the order of the extent of the bar minor axis (Athanassoula 1992a, figure 6). Thus, if the outer component of the CMC is linked to the x_2 family, its extent also should not exceed the size of the bar minor axis. This is not as easy to test as in the models of Athanassoula (1992a) because the bar isodensities are not simple ellipses. To test it we made images of the gas density in the inner part of the disc on which we superposed the isodensities of the combined DISK and STARS components (see the left panel of Fig. 6 for an example) and we created animations. By viewing both the individual images and the animations we were able to verify that our prediction is indeed born out.

8.4 Bar longevity

In our simulations bars never dissolved, even in cases with a very large fraction of gas. This is an important element in the debate on whether bars are long- or short-lived, because our simulations have live haloes, variable time-steps and a sufficient number of particles in all components to describe the evolution adequately. They thus should be giving the definitive answer, at least for the model we consider here. Furthermore, those with an initially large fraction of gas mass also form quite massive CMCs. As can be seen in Fig. 16, the CMC mass within a radius of one kpc from the centre can reach between 4 and 20 per cent of the total disc mass, depending on the total gas fraction. This is very considerable, but still does not suffice to dissolve the bar because the CMC extent is relatively large. Indeed – as has been shown both by orbital structure work (Hasan, Pfenniger, & Norman 1993) and by simulations (e.g. Shen & Sellwood 2004; Athanassoula et al. 2005) – for a given mass, the more compact the CMC, the more it will reduce the bar strength. If the same mass was concentrated within 100 pc rather than one kpc, it would dissolve the bar, but neither observed CMCs, nor those grown self-consistently in simulations are that compact.

Several other simulations with different initial condition models corroborate the fact that bars are long-lived. Villa-Vargas, Shlosman, & Heller (2010) use the same mass model as used here, but Berentzen et al. (2007) have different initial mass models. They also have a different description of the gas, namely with an isothermal equation of state with a temperature of 10^4 K, or, in a few cases, with an adiabatic equation of state. One of us

(EA) ran a series of simulations using a halo with a cusp, rather than a core as here, and still found long-lived bars. Moreover, bars are also found to be long-lived in the cosmological simulations of e.g. (Curir et al. 2006; Scannapieco & Athanassoula 2012, and in prep.) and particularly those of Kraljic et al. (2012), again with different mass models and different gas descriptions.

Thus, the evidence in favour of bars being long-lived in isolated galaxies is overwhelming. Could there, nevertheless, be exceptional cases where the bars could dissolve? Since the two studies in which bars did dissolve had rigid haloes, i.e. haloes which did not participate in the angular momentum redistribution within the galaxy, it makes sense to search in this direction, i.e. to make a simulation with a rigid halo in which the bar dissolved and repeat it identical except with a live halo, to see whether the bar still dissolves. A further clue can come from the fact that, as we showed in Sect. 4 that more flattened haloes inhibit bar growth during the secular evolution phase. Thus, the ideal candidate halo for allowing bar destruction would be a halo more squashed than $c/a=0.4$, i.e. disc-like, e.g. as advocated by Pfenniger, Combes & Martinet (1994). The physical relevance of such haloes, however, is not clear.

A more natural way of achieving bar destruction is via interactions. Indeed, several simulations (Pfenniger 1991; Athanassoula 1999; Berentzen et al. 2003) have shown that when a satellite galaxy falls in a disc galaxy, it can destroy a pre-existing bar, while the disc survives. This necessitates that the intruder is sufficiently dense to reach the central regions while its mass is still sufficiently high and also sets severe constraints on the geometry of the encounter. Bar destruction in such mergings can be easily understood because of the out-of-phase gravitational force the satellite exerts on the particles in the bar, preventing them from following the x_1 family of orbits, which is the backbone of the bar.

8.5 Comparison with observations. I

Figs. 4 and 5 show that, even for a single mass model, there is a variety of possible morphologies of the bar and its surrounding region. Comparing with images of observed galaxies, we see that all these morphologies are realistic, so that it is not possible to put any observational constraints from morphology alone. On the other hand, from the measurements of bar strength discussed in Sect. 4 and simple eye estimates of the bar length² from Figs. 4 and 5, or from the animations³, we see that our simulations give a very wide range of values, depending on the time, the gas fraction and the halo shape. Observations show a similar wide range of values, from the very strong bars such as NGC 4608 and 5701 discussed e.g. by Gadotti & de Souza (2003) and shown to be of the same strength as the bars in gas-less simulations, to the short and/or weak bars in SAB types.

In general, bars in gas-less simulations at times of the order of 10 Gyr or more, should have exceedingly strong bars. Indeed, both cosmological simulations (Kraljic et al. 2012) and observations (Sheth et al. 2008) argue that bars in very massive disc galaxies should be in place about 7 or 8 Gyr back, while bars in lower-mass, blue spirals should be in place later, perhaps as recently as 4

² For the present argument, simple eye estimates of the bar length are amply sufficient. More accurate measurements, using other methods, will be given elsewhere. Comparison between various methods of measuring bar lengths can be found in Athanassoula & Misiriotis (2002), Michel-Dansac & Wozniak (2006) and Gadotti et al. (2007).

³ <http://195.221.212.246:4780/dynam/movie/gtr>

or 5 Gyr ago. Applying these numbers here is not straightforward, because our simulations are dynamical and start only when the disc is fully formed, but, even so, it is clear that 10 Gyr is an overkill. Furthermore, discs do not form directly from stars. It is gas that rains in from the halo on to the disc where it forms stars. Thus, even galaxies whose discs at the present have very little gas, will have had much more at the time the bar started forming, so that studying bar formation in gas-less simulations is a further overkill. Therefore, bars in gas-less simulations at times of the order of 10 Gyr or more should be very long and strong, much more so than observed, so that when some gas is added and when shorter comparison times are considered, the bars become realistic. Thus the mass model we propose here fares well.

8.6 Comparison with observations. II

Our simulations help shed some light on the “downsizing” linked to bar formation. As already mentioned above, bars in massive, red disc galaxies are in place earlier than in blue, lower-mass spirals and the time difference is important, of the order of 1 to 3 Gyr, or more (Sheth et al. 2008; Kraljic et al. 2012). Sheth et al. (2008) tentatively brought up a possible explanation, namely that a low mass disc is more harassed by a given perturber than a very heavy one and that due to this harassment its bar can be destroyed. This holds clearly for the case of mergers, but not necessarily for the case of interactions, which can, on the contrary, drive rather than damp bars (Gerin et al. 1990; Miwa & Noguchi 2006; Berentzen et al. 2004). We will here propose an alternative explanation, but before discussing our alternative explanation, let us recall that observations show clearly that, both around redshift $z = 0$ and at intermediate redshifts, smaller galaxies have a larger fraction of gas than more massive ones (Erb et al. 2006; Daddi et al. 2010; Tacconi et al. 2010; Conselice et al. 2012).

Our explanation does not rely on interactions, but on the effect of gas. As we saw in Sect. 4, bars form faster in gas-less or gas-poor simulations than in gas-rich ones. This is due both to the fact that the initial simulation time during which the disc stays roughly axisymmetric is shorter (i.e. the bar starts growing earlier) and to the fact that, once it has started growing, the bar grows much faster. The two together argue strongly that bars will be in place in red galaxies much before they are in blue ones. Comparing two simulations identical in everything except for the gas-to-total mass ratio in the disc, we find that the difference between their bar formation times is in good agreement with what observations show us. Comparing e.g. simulations 101 and 111 we find that the former reaches a bar strength $A_2 = 0.3$ (0.4) before the latter with a time difference 2.1 (2.9) Gyr. This not only explains the delay, but also gives an estimate of the delay time which is in good agreement with observations. It can explain why bars are in place at earlier times in massive galaxies and at later times in blue, less massive ones. Of course, there are many differences between these two types of galaxies, other than the fraction of gas in the disc. These can include the total mass and extent of the galaxy, the form of its rotation curve and the existence of a bulge component. Nevertheless, our simulations argue that the effect of the gas can, by itself, go a long way towards accounting for the difference between bar formation times of red, massive galaxies and of blue, lower-mass ones.

8.7 Comparison with observations. III

Our work also introduces a number of further possibilities for confrontation with observations. For example, both a qualitative and

a quantitative comparison of the new morphological features, discussed in the end of Sect. 3.3 and Sect. 8.3, to analogous components in real galaxies would be very useful. Furthermore, thorough comparisons of the morphology of the observed gaseous CMC to our results in Sect. 3.4 should now be feasible with ALMA. In particular, it would be interesting to search for the existence of structures similar to those of the inner gaseous CMC. Indeed, as already mentioned, such a structure would only exist in galaxies with a core, so that the existence of such a structure would give further observational evidence for the existence of inner cores in galaxies and thus further input to the core versus cusp debate. On the other hand, the lack of such a structure would not necessarily point to a cusp.

A further, very worthwhile project is to study the kinematics of the halo stars located in the vicinity of the Galactic disc and this should be possible by comparing results from Sect. 6.4 with measurements from GAIA and from GAIA-related kinematical surveys on large ground-based telescopes. As already discussed, simulations show that the halo has a quite complex structure with in its inner part either a halo bar, or a close-to-axisymmetric region, depending on the bar strength. At larger distances from the centre the halo can stay triaxial. Analysis of the kinematics of a sufficient number of disc and halo stars of our Galaxy – as will be available from GAIA and from the related kinematical surveys on large ground-based telescopes – should shed light and set strong constraints on any theoretical study of the local disc/halo interaction. Inversely, any such theoretical study should allow us to explain and model these GAIA data.

9 SUMMARY AND CONCLUSIONS

In this paper we discussed the evolution of barred galaxies using simulations including gas and/or an initially triaxial halo. We showed that both the gas and the halo triaxiality influence strongly the bar formation, evolution and properties. In turn, the bar influences their properties and dynamics of its host galaxy, such as the gas surface density distribution, the halo shape and kinematics, as well as the redistribution of angular momentum within the galaxy.

In our simulations the gas fraction decreases with time due to star formation. Starting from a ratio of gas to total disc mass covering the whole range between 0% and 100%, it comes to levels well compatible with the fraction of gas in disc galaxies in the nearby universe, and at intermediate redshifts. Since our initial conditions were set up so as to be as near equilibrium as possible, in cases with initially strongly triaxial haloes both the DISK and the gas components start off non-axisymmetric, although less so than the halo. This lasts for at least one Gyr. During this time, the disc of young stars forms from the centre outwards, as expected, and both it and the gas show a clear multi-arm spiral structure.

9.1 Gas

In gas-rich discs, the disc stays near-axisymmetric much longer than in gas-poor cases, and, when the bar starts growing it does so at a much slower rate (Fig. 7). These two results, taken together, can explain the observation that bars are in place earlier in massive red disc galaxies than in blue spirals (Sheth et al. 2008). We also find that the morphological characteristics of both the gaseous and the stellar density distribution in the bar region are strongly influenced by the gas fraction.

A further important result is that the bar in gas-poor or gas-less cases grows to become longer and reaches a higher amplitude than in gas-rich cases, provided that the remaining parameter values are the same. We wish to stress, however, that increasing the gas fraction is not the only way to obtain this effect. Indeed, as already discussed in A03 for gas-less simulations, the length and strength of the bar are directly related to the angular momentum redistributed within the galaxy. The latter is influenced by the amount of angular momentum the halo can absorb, by the existence (or absence) of a classical bulge and its radial extent as well as the velocity anisotropy of all components (A03). Klypin et al. (2009) discussed the effect of the disc thickness. Here we added the effects of gas and halo shape, and their relative importance.

The bar in our simulations pushed the gas inwards to form a central mass concentration (CMC) with a very high gas density, resulting in considerable star formation. The mass of this CMC is in the range between 4 and 20 % of the total disc mass and it is more massive in more gas-rich simulations. In cases with an initially purely gaseous disc, its mass within the inner kpc can reach as high as $10^{10} M_{\odot}$. Thanks to the high resolution of our simulations, we were able to unravel the complex morphology of the gaseous CMC. We identified two components, a small inner one, elongated parallel to the bar, and a considerably larger one elongated perpendicular to it. Calculating orbits, we were able to show that this structure is due to a double ILR, the inner CMC being within the inner ILR and the outer one between the inner and the outer ILR.

A question which has been considerably debated over the last ten years or so, is whether bars are long-lived or short-lived. Indeed, a number of previous works have given conflicting results, but all of them had at least one caveat, concerning the number of gaseous particles, the spatial resolution and/or the appropriate description of halo resonances. Our simulations do not have either of these caveats and, furthermore, they have a resolution of 50 pc. In these simulations, we never witnessed any destruction or dissolution of a large scale bar, which strongly argues for long-lived bars, at least in isolated galaxies.

9.2 Halo

The effect of the halo relative mass on bar evolution is dual, as first discussed by Athanassoula (2002). Namely, during the early phases of bar formation the halo delays bar formation, while during the later secular evolution phase it makes the bar stronger. In this paper we showed that the effect of the halo shape on bar evolution is also dual. Thus, in the initial part of the evolution the non-axisymmetric forcing of the triaxial halo can trigger bar formation, so that bars in triaxial haloes grow earlier than in spherical ones. On the contrary, at the later stages of evolution, when the bar is well grown, halo triaxiality hinders bar growth due to the nonlinear interaction between the two non-axisymmetries. Thus in galaxies with strongly triaxial haloes bars grow earlier, but their strength hardly increases during the secular evolution phase.

We extend previous results on the halo bar (or dark matter bar) found in the innermost parts of the halo of gas-less models (e.g. Athanassoula 2005b, 2007; Colín et al. 2006) and we show that it also exists in gas rich models with initially spherical haloes and also in gas-less or gas-poor models with initially triaxial haloes. The inner parts of models with no halo bar show, on the contrary, an inner region which is more axisymmetric than the part outside it. Our simulations show that a very rough limit between the two types of models can be set by their bar strength, strong bars with

$A_2 > 0.5$ leading to a halo bar and weaker bars with $A_2 < 0.5$ leading to a halo inner part which is more axisymmetric than further out.

We also calculated the halo axial ratio in regions outside the halo bar. Using the region $10 > r > 30$ kpc, we find that the time evolution of the halo axial ratios is clearly linked to the time evolution of the bar strength. The strongest evolution occurs at times between bar growth and secular evolution.

There is a strong correlation between the bar strength and the amount of angular momentum absorbed by the halo, as has already been found for gas-less simulations with initially spherical haloes (A03). We find, however, that haloes with strong initial triaxiality, which stays strong during the simulation, deviate from this line following their own regression. This is in agreement with our results on the dual effect of the halo shape.

Part of the angular momentum absorbed by the halo changes considerably the halo kinematics and particularly that of the material near the disc equatorial plane, which acquires considerable rotation. This rotation correlates well with the bar strength and we find a Pearson correlation coefficient of the order of 0.9 between the maximum tangential velocity and the A_2 measure of the bar strength.

Another part of the angular momentum absorbed by the halo provides the halo with a bulk rotation, which is usually negligible over the first few Gyr and then increases steadily with time, contrary to that of the disc bar which decreases with time. Nevertheless, on average the position angle of the halo changes very little, of the order of $5^{\circ} - 30^{\circ}$ over a period of 10 Gyr. In general, we find larger rotations for initially strongly non-axisymmetric haloes and for low initial gas fractions (i.e. strong bars).

In models with triaxial haloes, a number of the main quantities describing the model – such as the bar strength, the halo axial ratios b/a and c/a , the angle of the major axis of the halo and of the gaseous CMC, etc – show clear oscillations in their time evolutions. These are due to the presence of several non-axisymmetric components, and they do not all rotate with the same pattern speed. We found that, to zeroth order approximation, when the bar and halo major axes are aligned, the A_2 has a minimum and the b/a has a maximum, i.e. in both cases the $m = 2$ components are less strong. On the contrary, when the bar and halo major axes are perpendicular, the A_2 has a maximum and the b/a has a minimum, i.e. the corresponding $m = 2$ components are stronger. Furthermore, the period of these variations is compatible with the relative frequency of the bar and halo rotation and the angles of the halo and of the gaseous CMC are also locked in the same oscillatory pattern.

ACKNOWLEDGEMENTS

It is a pleasure to thank Volker Springel for making available to us the version of GADGET2 used here, Albert Bosma and Arman Khalatyan for useful discussions and Jean-Charles Lambert for the uns and GLNEMO software (<http://projets.oamp.fr/projects/glnemo2>). EA acknowledges financial support to the DAGAL network from the People Programme (Marie Curie Actions) of the European Union's Seventh Framework Programme FP7/2007-2013/ under REA grant agreement number PITN-GA-2011-289313. EA also acknowledges financial support from the CNES (Centre National d'Etudes Spatiales - France). REGM acknowledges support from the Brazilian agencies FAPESP (05/04005-0) and CAPES (3981/07-0), and from the French Ministry of Foreign and European Affairs (Eiffel fellowship). SR acknowledges support from

the Russian Foundation for Basic Research (grants 08-02-00361-a and 09-02-00968-a) and a grant from the President of the Russian Federation for support of Leading Scientific Schools (grant NSH-1318.2008.2).

REFERENCES

- Abraham R. G., Tanvir N. R., Santiago B. X., Ellis R. S., Glazebrook K., van den Bergh S., 1996, *MNRAS*, 279, L47
- Abraham R. G., Merrifield M. R., Ellis R. S., Tanvir N. R., Brinchmann J., 1999, *MNRAS*, 308, 569
- Amorisco N. C., Evans N. W. 2012, *MNRAS*, 419, 184
- Aguerri J. A. L., Méndez-Abreu J., Corsini E. M., 2009, *A&A*, 495, 491
- Aguilar L. A., Merritt D., 1990, *ApJ*, 354, 33
- Allgood B., Flores R. A., Primack J. R., Kravtsov A. V., Wechsler R. H., Faltenbacher A., Bullock J. S., 2006, *MNRAS*, 367, 1781
- Athanassoula E., 1992a, *MNRAS*, 259, 328
- Athanassoula E., 1992b, *MNRAS*, 259, 345
- Athanassoula E., 1999, in *Astrophysical Discs*, ASP Conf. series Vol 160, J. A. Sellwood and Jeremy Goodman eds., 1999, p. 351
- Athanassoula E., 2002, *ApJL*, 569, L83
- Athanassoula E., 2003, *MNRAS*, 341, 1179 (A03)
- Athanassoula E., 2005a, *Cel. Mech. and Dyn. Astr.*, 91, 9
- Athanassoula E., 2005b, *MNRAS*, 358, 1477
- Athanassoula E., 2007, *MNRAS*, 377, 1569
- Athanassoula E., Bienaymé O., Martinet L. & Pfenniger D. 1983, *A&A*, 127, 349
- Athanassoula E., Lambert J. C., Dehnen W. 2005, *MNRAS*, 363, 496
- Athanassoula E., Misiriotis A., 2002, *MNRAS*, 330, 35
- Athanassoula E., Romero-Gómez M., Bosma A., Masdemont J.J. 2010, *MNRAS*, 407, 1433
- Bailin J., Steinmetz M., 2004, *ApJ*, 616, 27
- Bailin J., Steinmetz M., 2005, *ApJ*, 627, 647
- Barazza F.D., Jogee S., Marinova I., 2008, *ApJ*, 675, 1194
- Barnes J., Hut P., Goodman J., 1986, *ApJ*, 300, 112
- Battaglia G., Helmi A., Tolstoy E. 2008 et al., *ApJL*, 681, L13
- Beirão P., et al., 2012, *ApJ*, 751, 144
- Bellovary J. M., Dalcanton J. J., Babul A., Quinn T. R., Maas R. W., Austin C. G., Williams L. L. R., Barnes E. I., 2008, *ApJ*, 685, 739
- Berentzen I., Athanassoula E., Heller C. H., Fricke K. J., 2003, *MNRAS*, 341, 343
- Berentzen I., Athanassoula E., Heller C. H., Fricke K. J., 2004, *MNRAS*, 347, 220
- Berentzen I., Heller C. H., Shlosman I., Fricke K. J., 1998, *MNRAS*, 300, 49
- Berentzen I., Shlosman I., 2006, *ApJ*, 648, 807
- Berentzen I., Shlosman I., Jogee S., 2006, *ApJ*, 637, 582
- Berentzen I., Shlosman I., Martinez-Valpuesta I., Heller C. H., 2007, *ApJ*, 666, 189
- Binney J., Tremaine S., 1987, *Galactic Dynamics*. Princeton University Press
- Boily C. M., Athanassoula E., 2006, *MNRAS*, 369, 608
- Bournaud F., Combes F., 2002, *A&A*, 392, 83
- Bournaud F., Combes F., Semelin B., 2005, *MNRAS*, 364, L18
- Buta R. 1995, *ApJS*, 96, 39
- Buta R., Laurikainen E., Salo H., Knapen J. H., 2010, *ApJ*, 721, 259
- Cannizzo J. K., Hollister T. C., 1992, *ApJ*, 400, 58
- Ceverino D., Klypin A. 2007, *MNRAS*, 379, 1155
- Colín P., Valenzuela O., Klypin A., 2006, *ApJ*, 644, 687
- Conselice C., Mortlock A., Bluck A. F., Gruetzbauch R. 2012, arXiv:1206.6995
- Contopoulos G., 1980, *A&A*, 81, 198
- Contopoulos G., Papayannopoulos, T. 1980, *A&A*, 92, 33
- Curir A., Mazzei P., Murante G., 2006, *A&A*, 447, 453
- Daddi et al., 2010, *ApJ*, 713, 686
- Debattista V. P., Carollo C. M., Mayer L., Moore B., 2004, *ApJ*, 604, L93
- Debattista V. P., Mayer L., Carollo C. M., Moore B., Wadsley J., Quinn T., 2006, *ApJ*, 645, 209
- Debattista V. P., Moore B., Quinn T., Kazantzidis S., Maas R., Mayer L., Read J., Stadel J. A., 2008, *ApJ*, 681, 1076
- Debattista V. P., Sellwood J. A., 2000, *ApJ*, 543, 704
- Debattista V. P., Shen J., 2007, *ApJL*, 654, L127
- de Blok, W. J. G. 2010, *Advances in Astronomy*, 2010, article id. 789293
- de Blok, W. J. G., Bosma, A. 2002, *A&A*, 385, 816
- de Blok, W. J. G., Bosma, A., McGaugh, S. S. 2003, *MNRAS*, 340, 657
- de Blok, W. J. G., McGaugh, S. S., Bosma, A., Rubin, V. 2001, *ApJ*, 552, L23
- de Blok W. J. G., Walter F., Brinks E. et al. 2008, *AJ*, 136, 2648
- DeBuhr J., Ma C.-P., White S. D. M., 2012, *MNRAS*, 426, 983
- Dejonghe H., Merritt D., 1988, *ApJ*, 328, 93
- de Vaucouleurs G., de Vaucouleurs A., Corwin H. G. Jr., Buta R. J., Paturel G., Fouque P., 1991, *Third Reference Catalogue of Bright Galaxies*, New York, Springer (RC3)
- Dubinski, J. 1994, *ApJ*, 431, 617
- Dubinski J., Berentzen I., Shlosman I. 2009, *ApJ*, 697, 293
- Dubinski J., Carlberg R. G., 1991, *ApJ*, 378, 496
- El-Zant A., Shlosman I. 2002, *ApJ*, 577, 626
- Elmegreen B. G., Elmegreen D. M., Hirst A.C., 2004, *ApJ*, 612, 191
- Erb D. K., Steidel C. C., Shapley A. E., Pettini M., Reddy N. A., Adelberger K. L. 2006, *ApJ*, 646, 107
- Eskridge P. B., et al., 2000, *AJ*, 119, 536
- Gadotti D. A., 2011, *MNRAS*, 415, 3308
- Gadotti D. A., Athanassoula E., Carrasco L., Bosma A., de Souza R. E., Recillas E., 2007, *MNRAS*, 381, 943
- Gadotti D. A., de Souza R. E., 2003, *ApJL*, 583, L75
- Gerin M., Combes F., Athanassoula E. 1990, *A&A*, 230, 37
- Gnedin O., Kravtsov, A., Klypin, A., Nagai D., 2004, *ApJ*, 616, 16
- Hasan H., Pfenniger D., Norman C., 1993, *ApJ*, 409, 91
- Heller C. H., Shlosman I., Athanassoula E., 2007a, *ApJ*, 657, L65
- Heller C. H., Shlosman I., Athanassoula E., 2007b, *ApJ*, 671, 226
- Heller C. H., Shlosman I., Englmaier P., 2001, *ApJ*, 553, 661
- Hernquist L., 1993, *ApJS*, 86, 389
- Hernquist L., Weinberg M., 1992, *ApJ*, 400, 80
- Holley-Bockelmann K., Weinberg J. C., Katz S., 2005, *MNRAS*, 363, 991
- Hoyle B., et al., 2011, *MNRAS*, 415, 3627
- Huss A., Jain B., Steinmetz M., 1999, *ApJ*, 517, 64
- Jing Y. P., Suto Y., 2002, *ApJ*, 574, 538
- Jog C. J., 2000, *ApJ*, 542, 216
- Jog C. J., Solomon P. M., 1984, *ApJ*, 276, 114
- Jogee S. et al., 2004, *ApJ*, 615, 105
- Kazantzidis S., Kravtsov A. V., Zentner A. R., Allgood B., Nagai D., Moore B., 2004, *ApJL*, 611, L73

- Klypin A., Valenzuela O., Colin, P., Quinn T. 2009, MNRAS, 398, 1027
- Knapen J., Shlosman I., Peletier R., 2000, ApJ, 529, 93
- Kormendy J., Kennicutt R. C., Jr., 2004, ARA&A, 42, 603
- Kraljic K., Bournaud F., Martig M. 2012, ApJ, 757, 60
- Kuzio de Naray R., McGaugh S. S., de Blok W. J. G., Bosma A. 2006, ApJS, 165, 461
- Kuzio de Naray R., McGaugh S. S., de Blok W. J. G. 2008, ApJ, 676, 920
- Lambas D. G., Maddox S. J., Loveday J., 1992, MNRAS, 258, 404
- Laurikainen E., Salo H., Buta R., 2004, ApJ, 607, 103
- Laurikainen E., Salo H., Buta R., Knapen J. H., 2011, MNRAS, 418, 1452
- Leroy A. K., Walter F., Brinks E., Bigiel F., de Blok W. J. G., Madore B., Thornley M. D., 2008, AJ, 136, 2782
- Machado R. E. G., Athanassoula E., 2010, MNRAS, 406, 2386
- Maciejewski W., Athanassoula E., 2007, MNRAS, 380, 999
- Maciejewski W., Sparke L. S., 1997, ApJ, 484, L117
- Maciejewski W., Sparke L. S., 2000, MNRAS, 313, 745
- MacMillan J. D., Widrow L. M., Henriksen R. N., 2006, ApJ, 653, 43
- Marinova I., Jogee S., 2007, ApJ, 659, 1176
- Marinova I. et al., 2009, ApJ, 698, 1639
- Martin P., 1995, AJ, 109, 2428
- Martínez-García E. E., 2012, ApJ, 744, 92
- Martínez-Valpuesta I., Shlosman I., Heller C., 2006, ApJ, 637, 214
- Masters K. L., et al., 2011, MNRAS, 411, 2026
- McMillan P. J., Athanassoula E., & Dehnen W. 2007, MNRAS, 376, 1261
- Méndez-Abreu J., Sánchez-Janssen R., Aguerri J. A. L., 2010, ApJ, 711, L61
- Menéndez-Delmestre K., Sheth K., Schinnerer E., Jarrett T. H., Scoville N. Z., 2007, ApJ, 657, 790
- Merritt D., & Aguilar L. A. 1985, MNRAS, 217, 787
- Michel-Dansac L., Wozniak H. 2006, A&A, 452, 97
- Miwa T., Noguchi M. 1998, ApJ, 499, 149
- Nair, P. B., & Abraham, R. G. 2010, ApJL, 714, L260
- Navarro, J. F., Frenk, C. S., White, S. D. M. 1996, ApJ, 462, 563
- Nordström, B., et al. 2004, A&A, 418, 989
- Norman C. A., Sellwood J. A., Hasan H., 1996, ApJ, 462, 114
- Novak G. S., Cox T. J., Primack J. R., Jonsson P., Dekel A., 2006, ApJL, 646, L9
- Oh S.-H., de Blok W. J. G., Walter F., Brinks E., Kennicutt, R. C. Jr. 2008, AJ, 136, 2761
- O'Neill J. K., Dubinski J., 2003, MNRAS, 346, 251
- Patsis P. A., Athanassoula E., 2000, A&A, 358, 45
- Peñarrubia J., Pontzen A., Walker M. G., Koposov S. E., 2012, ApJ, 759, L42
- Pérez I., Aguerri J. A. L., Méndez-Abreu J., 2012, A&A, 540, A103
- Pfenniger, D. 1991 in *Dynamics of Disc Galaxies*, eds. B. Sundelius. Göteborgs: Göteborgs University and Chalmers, p. 191
- Pfenniger D., Combes F., Martinet L. 1994, A&A, 285, 79
- Prada F., Klypin A., Cuesta A., Betancort-Rijo J., Primack J. 2012, MNRAS, 423, 3018
- Press W. H., Teukolsky S. A., Vetterling W. T., Flannery B. P., 1992, in *Numerical Recipes*, Cambridge University Press, Cambridge
- Rautiainen, P., Salo, H., Laurikainen, E. 2002, MNRAS, 337, 1233
- Rodionov S. A., Athanassoula E., 2011, A&A, 529, A98
- Rodionov S. A., Athanassoula E., Sotnikova N. Y., 2009, MNRAS, 392, 904
- Saha, K., Martínez-Valpuesta I., Gerhard O. 2012, mnras, 421, 333
- Scannapieco C., Athanassoula E., 2012, MNRAS, 425, L10
- Sanders, R. H., Huntley, J. M. 1976, ApJ, 209, 53
- Scannapieco C., et al., 2012, MNRAS, 423, 1726
- Schneider M. D., Frenk C. S., Cole S., 2012, JCAP, 5, 30
- Shen V., Sellwood L., 2004, ApJ, 604, 614
- Sheth K., Vogel S. N., Regan M. W., Thornley M. D., Teuben P. J., 2005, ApJ, 632, 217
- Sheth K. et al. 2008, ApJ, 675, 1141
- Simard L., Mendel J. T., Patton D. R., Ellison S. L., McConnachie A. W., 2011, ApJS, 196, 11
- Simon J. D., Bolatto A. D., Leroy A., Blitz L. 2003, ApJ, 596, 957
- Springel V., Hernquist L., 2002, MNRAS, 333, 649
- Springel V., Hernquist L., 2003, MNRAS, 339, 289
- Springel V., 2005, MNRAS, 364, 1105
- Springel V., Yoshida N., White S. D. M., 2001, NewA, 6, 79
- Springel V., Di Matteo T., Hernquist L., 2005, MNRAS, 361, 776
- Tacconi L. et al. 2010, Nature, 463, 781
- Trachternach C., de Blok W. J. G., Walter F., Brinks E., Kennicutt R. C., 2008, AJ, 136, 2720
- Toomre A., 1964, ApJ, 139, 1217
- Valenzuela O., Klypin A., 2003, MNRAS, 345, 406
- Valluri M., Debattista V. P., Quinn T., Moore B., 2010, MNRAS, 403, 525
- van den Bergh S., Abraham R. G., Ellis R.S., Tanvir N. R., Santiago B., Glazebrook K. G., 1996, AJ, 112, 359
- Vera-Ciro C. A., Sales L. V., Helmi A., Frenk C. S., Navarro J. F., Springel V., Vogelsberger M., White S. D. M., 2011, MNRAS, 416, 1377
- Villa-Vargas J., Shlosman I., Heller C., 2010, ApJ, 719, 1470
- Walker M. G., Peñarrubia J. 2012, ApJ, 742, 20
- Wang J., et al., 2012, arXiv:1205.0932
- Warren M. S., Quinn P. J., Salmon J. K., Zurek W. H., 1992, ApJ, 399, 405
- Weinberg M. D., 1991, ApJ, 368, 66
- Whyte L. F., Abraham R. G., Merrield M. R., Eskridge P. B., Frogel J. A., Pogge R.W., 2002, MNRAS, 336, 1281
- Widrow L. M., 2008, ApJ, 679, 1232
- Wozniak H., Michel-Dansac L., 2009, A&A, 494, 11